15. SITE 939[1]

Shipboard Scientific Party[2]

HOLE 939A

Date occupied: 1 May 1994

Date departed: 2 May 1994

Time on hole: 14 hr, 45 min

Position: 4°43.308′N, 47°30.201′W

Bottom felt (drill pipe measurement from rig floor, m): 2794.8

Distance between rig floor and sea level (m): 11.23

Water depth (drill pipe measurement from sea level, m): 2783.6

Penetration (m): 102.70

Number of cores (including cores having no recovery): 11

Total length of cored section (m): 102.70

Total core recovered (m): 97.57

Core recovery (%): 95

Oldest sediment cored:
   Depth (mbsf): 102.70
   Nature: Silty clay
   Earliest age: Pleistocene

HOLE 939B

Date occupied: 2 May 1994

Date departed: 2 May 1994

Time on hole: 12 hr, 30 min

Position: 4°43.305′N, 47°29.940′W

Bottom felt (drill pipe measurement from rig floor, m): 2803.5

Distance between rig floor and sea level (m): 11.23

Water depth (drill pipe measurement from sea level, m): 2792.3

Penetration (m): 99.40

Number of cores (including cores having no recovery): 11

Total length of cored section (m): 99.40

Total core recovered (m): 99.51

Core recovery (%): 100

Oldest sediment cored:
   Depth (mbsf): 99.40
   Nature: Silty clay
   Earliest age: Pleistocene

HOLE 939C

Date occupied: 2 May 1994

Date departed: 2 May 1994

Time on hole: 8 hr, 30 min

Position: 4°43.307′N, 47°29.944′W

Bottom felt (drill pipe measurement from rig floor, m): 2802.4

Distance between rig floor and sea level (m): 11.26

Water depth (drill pipe measurement from sea level, m): 2791.1

Penetration (m): 36.10

Number of cores (including cores having no recovery): 4

Total length of cored section (m): 36.10

Total core recovered (m): 36.98

Core recovery (%): 102

Oldest sediment cored:
   Depth (mbsf): 36.10
   Nature: Silty clay
   Earliest age: Pleistocene

Principal results: Site 939 (proposed Site AF-12) is located about 1.0–1.5 km east of the crest of the eastern levee of the Amazon Channel on the upper Amazon Fan. It is one of a series of sites located on the flank of the Amazon Channel intended to study the late-glacial/early-interglacial evolution of the fan channel and changes in organic-matter diagenesis and pore-water chemistry. The 480-m offset of Holes 939A and 939B provides an opportunity to study lateral variability in upper-fan overbank turbidites.

The site was selected from a *Conrad* 3.5-kHz profile (C2514; 0837 hr on 8 Dec. 1984). Hole 939A was located about 480 m to the west of Holes 939B and 939C to assess the lateral variability in sedimentation. Hole 939C was used for detailed geochemical and paleontological sampling.

Hole 939A was cored by APC to 83.7 mbsf, then by XCB to 102.7 mbsf, with total sediment recovery of 97.57 m (95.0%). Hole 939B was cored by APC to 80.0 mbsf, then by XCB to 99.4 mbsf, with total recovery of 99.51 m (100.1%). Hole 939C was cored to 36.1 mbsf and recovered 36.98 m (102.4%).

Temperature measurements were made at 51 and 80 mbsf (ADARA) in Hole 939B, indicating a mean geothermal gradient of 29°C/km. There was gas expansion in all cores. Methane was found throughout the hole, but higher hydrocarbons were not detected.

Two lithologic units are recognized (using Hole 939B as a type section):

Unit I (0–0.68 mbsf) is a Holocene bioturbated foraminifer-nannofossil clay, underlain by an iron-rich crust and a gray nannofossil-rich clay.

Unit II (0.68–99.40 mbsf) consists of mud with interbedded laminae and beds of silt and very fine sand. The mud has a carbonate content of <3%. Most of the unit is stained by diagenetic hydrotroilite in irregular patches or color bands. Small soft nodules of hydrotroilite, 1–2 mm in diameter, are common, and larger concretions and continuous bands are present from 8 to 16 mbsf. The unit is subdivided into five subunits, based
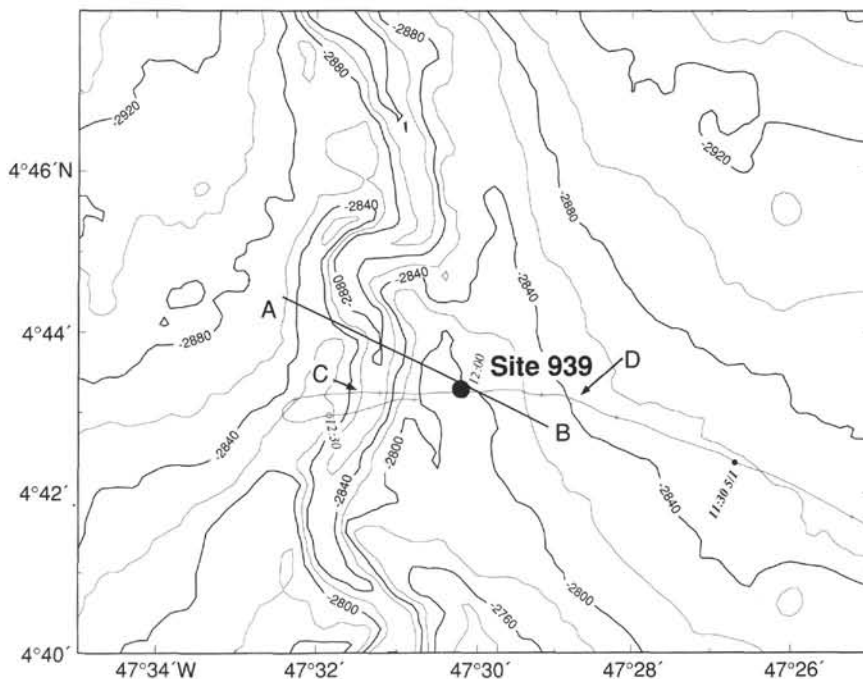
Figure 1. Location of Site 939 showing *JOIDES Resolution* and *Conrad* tracks. A–B is 3.5-kHz profile in Figure 2; C–D is 3.5-kHz profile in Figure 3. Bathymetry in meters.

mainly on the frequency of silt laminae and beds. Subunit IIA (0.68–23.00 mbsf) comprises bioturbated mud. A prominent change in reflection character seen at 15 mbsf on 3.5-kHz profiles appears to form a seismic discontinuity but has no corresponding lithologic change other than common 1- to 2-cm hydrotroilite nodules. Subunit IIB (23.00–44.23 mbsf) consists of moderately bioturbated mud with laminae and thin beds of silt. Burrows cut and obliterate parts of silt layers. Subunit IIC (44.23–66.17 mbsf) consists mainly of moderately bioturbated mud, with one short interval with many silt laminae. Subunit IID (66.17–81.50 mbsf) resembles Subunit IIB, except for a greater frequency of silt laminae and beds. Subunit IIE (81.50–99.4 mbsf) consists of mud with some color banding, rare silt laminae, and structureless mud turbidites.

Hole 939A was located 480 m west of Hole 939B, closer to the levee crest. The sediment sequence thickens toward the levee crest, and lithostratigraphic boundaries near the bottom of Hole 939A are about 13 m deeper than in Hole 939B. Both the number and thickness of silt beds decrease away from the channel.

Foraminifer abundances are generally low below Subunit IIA. *P. obliquiloculata* is not present below the Holocene, indicating an age <40 ka for Unit II. Unit I and Subunit IIA contain pteropods. Echinoid spines occur from 24 to 80 mbsf. Rare abyssal benthic foraminifers are present in Subunits IIA and IID.

No paleomagnetic excursion was found at this site. In Hole 939A, variation in magnetic inclination, interpreted as secular variation, was detected between 3 and 35 mbsf, with a short 1- to 2-m wavelength variation superimposed on a longer 8- to 20-m wavelength variation. There are three well-defined oscillations in declination over a range of 90° from 20 to 60 mbsf and two oscillations of <35° between 70 and 80 mbsf.

Physical-properties data suggest that the site experienced normal compaction, except for an interval from 17 to 27 mbsf, where compaction was inhibited and shear strength is low.

At Hole 939C, interstitial waters were collected at 1.5-m intervals to 18.5 mbsf and thereafter at 3-m intervals to 37 mbsf. Samples were also taken every 20 m in Hole 939B. Magnesium and calcium decrease from 55 mM (Mg) and 12 mM (Ca) at 0.2 mbsf to about 43 mM (Mg) and 4 mM (Ca) near 30 mbsf, thereafter remaining almost constant. Mg and Ca concentrations correlate well, suggesting that their loss from the pore water is related. Pore-water sulfate diminishes from 27 mM at 0.2 mbsf to 21 mM at 1.4 mbsf and to zero by 9 mbsf. Alkalinity increases rapidly to 31 mM

at 9 mbsf and then decreases to 10 mM at 40 mbsf, remaining constant below that. Balancing possible sources and sinks of alkalinity suggests that almost all alkalinity removed from pore fluids can be accounted for as Ca or Mg carbonate. Pore-water phosphate peaks at 98 mM, at the depth of complete sulfate reduction (9 mbsf). Dissolved iron is between 56 and 94 mM in the upper 33 mbsf, reaches a peak of 326 mM at 42 mbsf, and then decreases to 143 mM at 73 mbsf. Organic carbon ranges from 1.0% to 0.8% in Unit II. No discrete carbonate phases have been identified in the cores, although 1%–3% carbonate is present in mud samples. Vivianite (iron phosphate) nodules are common and displace surrounding sediment, crosscutting earlier-formed iron monosulfides that fill pore space. Organic-carbon concentration is almost constant through the interval of detailed pore-water study. Slight changes in elemental compositions may be related to diagenetic changes, such as low nitrogen values (<0.07%) at 0.5–8.0 mbsf, which could indicate preferential oxidation of reactive nitrogenous organic compounds.

This site represents one of the highest near-surface sedimentation rates on Leg 155. The upper part of the pore-water profile (to 5 mbsf) is similar to that at Site 931, where the sedimentation rate is several times lower, but the peaks in phosphate and iron are several meters deeper than at Site 931. Fluctuations in the deposition of silt beds on the upper fan occur with a period estimated to be on the order of hundreds to a few thousands of years.

SETTING AND OBJECTIVES

Introduction

Site 939 (proposed Site AF-12) is a series of three shallow holes located on the flank of the Amazon Channel intended to study the late-glacial/early-postglacial evolution of the upper fan channel (water depth 2794 mbsl), lateral variability in upper-fan sediment, organic matter diagenesis, and pore-water chemistry.

Setting

Site 939 is located on the eastern (right) flank of the Amazon Channel about 7 m below the adjacent levee crest (Fig. 1). SeaBeam bathymetric data in this area suggest that the channel shape evolved
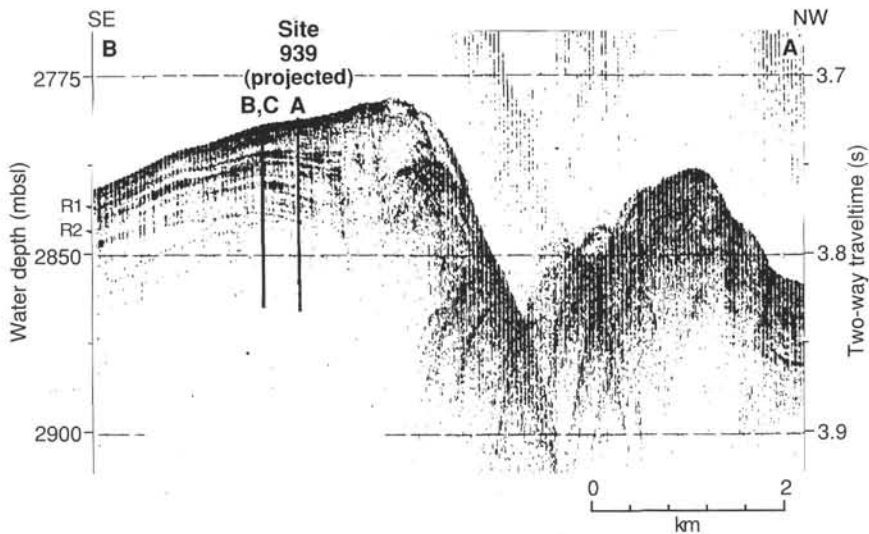
Figure 2. A 3.5-kHz profile from *Conrad* near Site 939. R1 and R2 are reflections discussed in text. Location shown as A–B in Figure 1.

from more to less sinuous as the sediment supply to the fan reduced (Pirmez, 1994). The 3.5-kHz profile in this area (Fig. 2) shows a change from weak to strong reflections downsection that is suggestive of a change in sediment characteristics. Our initial interpretation was that this change in reflection strength is due to the same change in sedimentation that caused the increasing sinuosity. This site, Site 937, and Site 938 are the shallowest-water sites drilled during Leg 155.

The site was selected from a *Conrad* 3.5-kHz profile (C2514; 0837 hr on 8 Dec. 1984; Fig. 2). Our pre-site 3.5-kHz survey verified the reflection sequence (Fig. 3), although the deeper reflections were not seen because of sea state. The beacon site was chosen at 1200UTC on 1 May 1994 on our *JOIDES Resolution* profile. This appears to be equivalent to the position initially selected on the *Conrad* line. Hole 939A is located about 480 m west of Holes 939B and 939C to allow an assessment of lateral variability in sediment layering.

The surficial sediment at the site, interpreted from sub-bottom and seismic profiles, include a layer of weakly stratified sediment 15–30 m thick overlying a series of stronger reflections, the top of which is identified as R1 on Figs. 2 and 3. Closer to the levee crest, the upper

and lower units are difficult to discern as both are transparent, presumably because sediment layering is complex. Overall, the levee crest appears to have prograded toward the channel during aggradation. A prominent reflection (R1) at 18 ms at Hole 939B marks the base of the relatively transparent upper interval that thickens to 22 ms at Hole 939A and to 28 ms at the levee crest (Fig. 3). This reflection dips away from the channel east of Hole 939A and is almost horizontal to the west of Hole 939A. Underlying reflections appear to toplap against this reflection R1 (Fig. 2). These deeper reflections dip toward the channel west of Hole 939B and away from the channel to the east of Hole 939B. A second reflection with underlying toplap is seen at 32 ms at Hole 939B (R2 in Fig. 2).

Objectives

The principal objectives at Site 939 were:

1. To determine the nature of levee sediment, and especially changes that would correlate with reflectivity and/or observed bathymetric patterns.
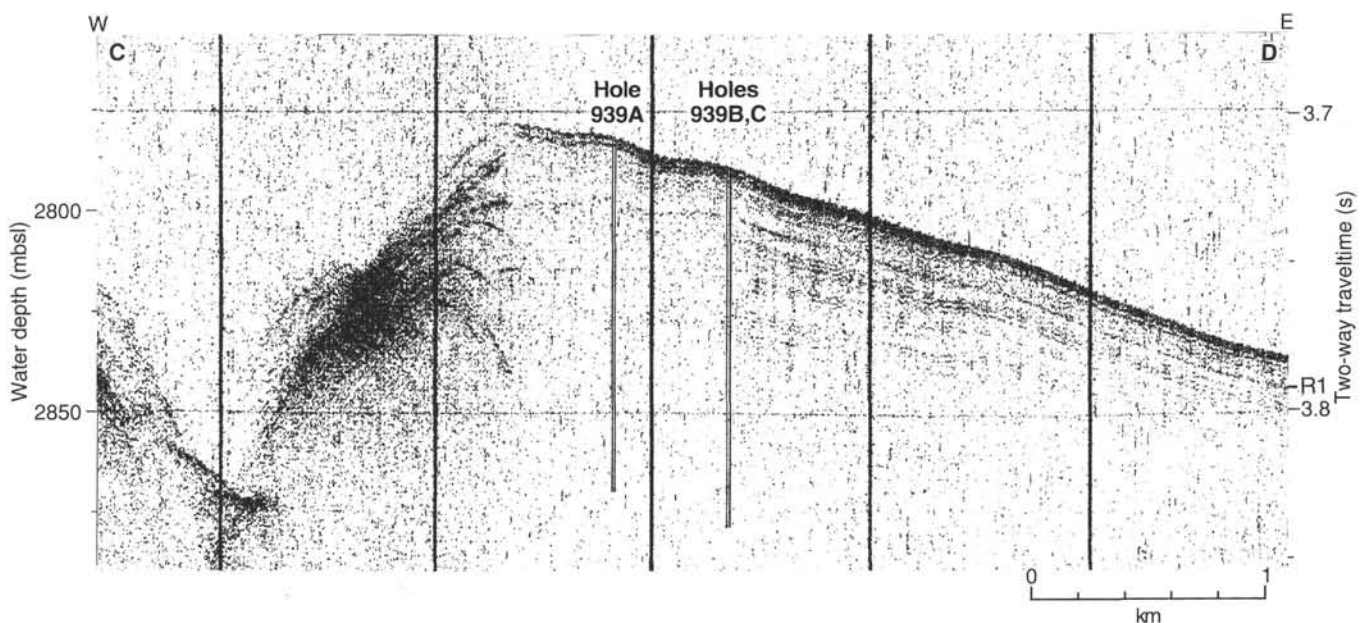

Figure 3. A 3.5-kHz profile from *JOIDES Resolution* through Site 939. R1 is reflection discussed in text. Location shown as C–D in Figure 1.

Table 1. Site 939 coring summary.

Core	Date (1994)	Time (UTC)	Depth (mbsf)	Length cored (m)	Length recovered (m)	Recovery (%)
155-939A-						
1H	May 1	1905	0.0–7.7	7.7	7.68	99.7
2H	May 1	1940	7.7–17.2	9.5	9.82	103.0
3H	May 1	2020	17.2–26.7	9.5	9.18	96.6
4H	May 1	2105	26.7–36.2	9.5	10.08	106.1
5H	May 1	2150	36.2–45.7	9.5	9.54	100.0
6H	May 1	2230	45.7–55.2	9.5	11.16	117.5
7H	May 1	2315	55.2–64.7	9.5	9.82	103.0
8H	May 2	0015	64.7–74.2	9.5	9.57	101.0
9H	May 2	0100	74.2–83.7	9.5	9.85	103.0
10X	May 2	0215	83.7–93.2	9.5	7.85	82.6
11X	May 2	0315	93.2–102.7	9.5	3.02	31.8
Coring totals				102.7	97.6	95.00
155-939B-						
1H	May 2	0550	0.0–4.0	4.0	4.00	100.0
2H	May 2	0630	4.0–13.5	9.5	9.43	99.2
3H	May 2	0725	13.5–23.0	9.5	10.43	109.8
4H	May 2	0805	23.0–32.5	9.5	10.13	106.6
5H	May 2	0855	32.5–42.0	9.5	10.58	111.3
6H	May 2	1000	42.0–51.5	9.5	10.29	108.3
7H	May 2	1045	51.5–61.0	9.5	10.51	110.6
8H	May 2	1135	61.0–70.5	9.5	8.54	89.9
9H	May 2	1300	70.5–80.0	9.5	9.93	104.0
10X	May 2	1430	80.0–89.7	9.7	7.50	77.3
11X	May 2	1530	89.7–99.4	9.7	8.17	84.2
Coring totals				99.4	99.5	100.10
155-939C-						
1H	May 2	1700	0.0–7.6	7.6	7.60	100.0
2H	May 2	1740	7.6–17.1	9.5	10.05	105.8
3H	May 2	1815	17.1–26.6	9.5	9.00	94.7
4H	May 2	1900	26.6–36.1	9.5	10.33	108.7
Coring totals				36.1	37.0	102.40

Note: An expanded version of this coring summary table that includes lengths and depths of sections, location of whole-round samples, and comments on sampling disturbance is included on the CD-ROM in the back pocket of this volume.

2. To characterize lateral variability in sediment characteristics within upper levee sediment through sampling at two offset holes.
3. To determine pore-water chemistry and related changes in the diagenesis of organic matter through a high-resolution pore-water and sediment chemistry sampling program.

OPERATIONS

Transit: Site 938 to Site 939 (AF-12)

We transited 10 nmi from Site 938 to Site 939 (AF-12) in 0.9 hr and conducted a seismic-reflection survey over the site. At 0921 hr 1 May, we deployed a beacon at 4°43.307′N, 47°30.110′W.

Hole 939A

We offset the ship about 250 m east of the beacon and assembled a BHA similar to that used at Site 938. We positioned the bit at 2793.0 mbrf and spudded Hole 939A at 1450 hr 1 May. The distance from sea level to rig floor, which depends on the ship's draft, was 11.23 m for Holes 939A and 939B, and 11.26 m for Hole 939C. Core 1H recovered 7.68 m of sediment, and the mud line was defined to be at 2794.8 mbrf. Cores 1H through 9H were taken from 2794.8 to 2878.5 mbrf (0–83.7 mbsf), recovering 86.70 m (103%; Table 1). Cores 4H through 9H were oriented using the Tensor tool. No heat-flow measurements were made. Overpull was 40,000 lb while retrieving Core 9H from the formation.

XCB Cores 10X and 11X were taken from 2878.5 to 2897.5 mbrf (83.7–102.7 mbsf), coring 19.0 m and recovering 10.87 m of sediment (57%). The overall APC/XCB recovery was 95%. Parts of

Table 2. Stratigraphically equivalent depths in Holes 939A and 939B of 3.5-kHz reflections, lithologic boundaries, and peaks in magnetic susceptibility (see Figs. 4 and 20).

	Depth (mbsf)	
Features	Hole 939A	Hole 939B
3.5-kHz picks	16	12
	33	26
	47	37
Lithologic boundaries		
Base of Subunit IIA	24.45	23.00
Base of Subunit IIB	54.48	44.23
Top silt packet, Subunit IIC	64.85	53.34
Base of Subunit IIC	78.73	66.17
Magnetic susceptibility peaks		
a	9.00	7.64
b	20.71	15.93
c	24.44	19.39
d	40.99	33.34
e	44.04	36.24
f	56.10	45.60
g	59.77	48.35
h	64.94	52.16
i	67.29	53.91
j	70.09	59.36
k	79.57	64.70
l	82.88	67.09
m	89.40	76.70
n (?)	95.39	87.14

Cores 2H, 3H, 6H, and 7H were disturbed as a result of either gas-induced extrusion of core from the liner onto the rig floor or collapsed core liners.

Hole 939B

We offset the ship about 500 m east of Hole 939A, positioned the bit at 2798.0 mbrf, and spudded Hole 939B at 0137 hr 2 May. Core 1H recovered 4.00 m, and the mud line was defined to be at 2803.5 mbrf. Cores 1H through 9H were taken from 2803.5 to 2883.5 mbrf (0–80.0 mbsf) and recovered 83.84 m (105%). Cores 3H through 9H were oriented using the Tensor tool. ADARA heat-flow measurements were taken during Cores 6H and 9H. The core barrel only partially stroked while taking Core 9H and required overpull of 70,000 lb to retrieve it from the formation.

XCB Cores 10X and 11X were taken from 2883.5 to 2902.9 mbrf (80.0–99.4 mbsf), coring 19.4 m and recovering 15.67 m (80.8% recovery). The overall APC/XCB recovery was 100.1%. Parts of Cores 3H, 8H, and 9H were disturbed as a result of either gas-induced extrusion of core from the liner onto the rig floor or collapsed core liners.

Hole 939C

We offset the ship about 20 m west of Hole 939B, positioned the bit at 2800.5 mbrf, and spudded Hole 939C at 1250 hr 2 May. Core 1H recovered 7.60 m, and the mud line was defined to be at 2802.4 mbrf. Cores 1H through 4H were taken from 2802.4 to 2838.5 mbrf (0–36.1 mbsf) and recovered 36.98 m (102.4%). No cores were oriented and no heat-flow measurements were made. Part of Core 3H was disturbed as a result of a collapsed core liner. The bit cleared the rig floor at 2100 hr 2 May, and we retrieved the beacon.

LITHOSTRATIGRAPHY

Introduction

Holes 939A, 939B, and 939C penetrate upper Quaternary sediment at the crest of the eastern levee of the Amazon Channel. Hole
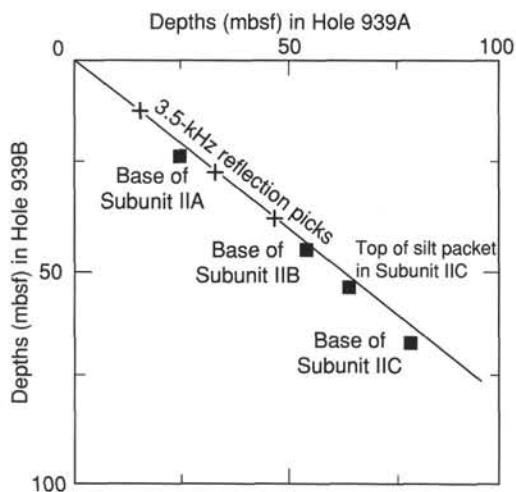
Figure 4. Stratigraphically equivalent depths in Holes 939A and 939B. The solid line is based on three picks (+ symbols) of the depth to equivalent 3.5-kHz reflections in Figure 3, using an assumed sound velocity of 1500 m/s. Boxes show the corresponding depths of lithologic boundaries (Table 2).

939C (0 to 36.1 mbsf) is adjacent to Hole 939B and duplicates the upper part of the section recovered in Hole 939B. Hole 939A is about 2 km east of the channel axis and 1 km east of the levee crest. Holes 939B and 939C are about 480 m east of Hole 939A.

Differential sediment accumulation between Holes 939A and 939B suggests that equivalent features should be encountered at shal-

lower sub-bottom depths in Hole 939B than in Hole 939A (see "Setting and Objectives" section, this chapter). This differential accumulation is verified by the depths to the boundaries of lithostratigraphic units and by correlation of magnetic susceptibility data for Holes 939A and 939B (Table 2; Fig. 4 and Fig. 20). Thus, lithostratigraphic boundaries near the bottom of Hole 939B are about 13 m shallower than in Hole 939A, and Cores 939B-10X and -11X sample older intervals than did the deepest recovery in Hole 939A.

In the lithostratigraphic summary that follows, sub-bottom depths of unit boundaries are given for both Holes 939A and 939B where they are different. The succession in Hole 939C is not described separately because it is essentially the same as in Hole 939B. Individual laminae and thin beds of silt could not be unambiguously correlated between Holes 939B and 939C, but groups of silt layers occur at essentially the same depth in the two holes, plus or minus about 30 cm.

The composite lithologic section (Fig. 5) is based on Hole 939B. The graphic sedimentological column (Fig. 6) is mainly based on the expanded section in Hole 939A that was less disturbed during coring. In the sedimentological columns, Cores 939B-8H through -11X are plotted with a different depth scale than the cores from Hole 939A, using the top of Subunit IID as a datum (78.73 mbsf in Hole 939A; 66.17 mbsf in Hole 939B). Core 939A-11X had poor recovery and is not shown in the sedimentological column.

Expansion of methane gas during core recovery commonly affected the sediment by disrupting the primary sedimentary structures in many silt beds and by producing void spaces within many of the core sections (see "Lithostratigraphy" section in the "Explanatory Notes" chapter, this volume). Coring disturbance and broken core liners in several APC cores precluded detailed description of these sections (Cores 939A-7H and -9H; Cores 939B-8H and -9H).
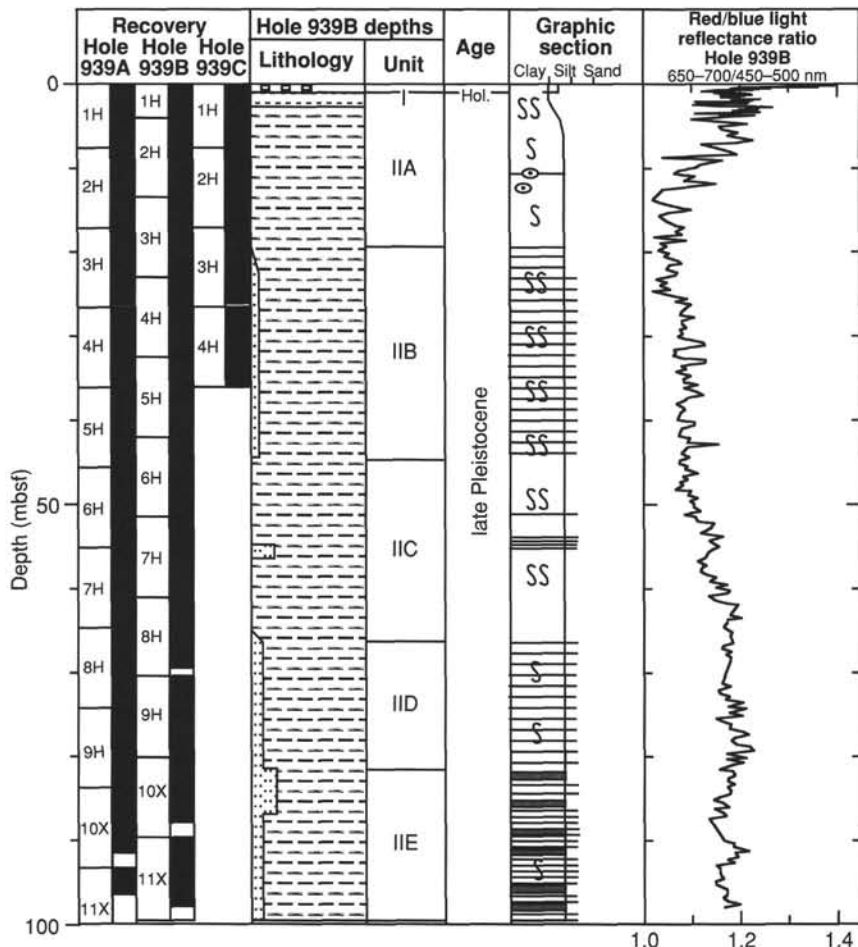
Figure 5. Composite stratigraphic section for Site 939 showing core recovery in all holes, a simplified summary of lithology for Hole 939B, depths of unit boundaries in Hole 939B, a graphic section with generalized grain size and bedding characteristics, and downhole variations in light-reflectance values for cores from Hole 939B only. The lithologic symbols are explained in Figure 1 of the "Explanatory Notes" chapter, this volume. At this site, unit boundaries have quite different depths in Holes 939A and 939B (see text and Fig. 4). The depths of unit boundaries in Hole 939A are available in Figure 6.
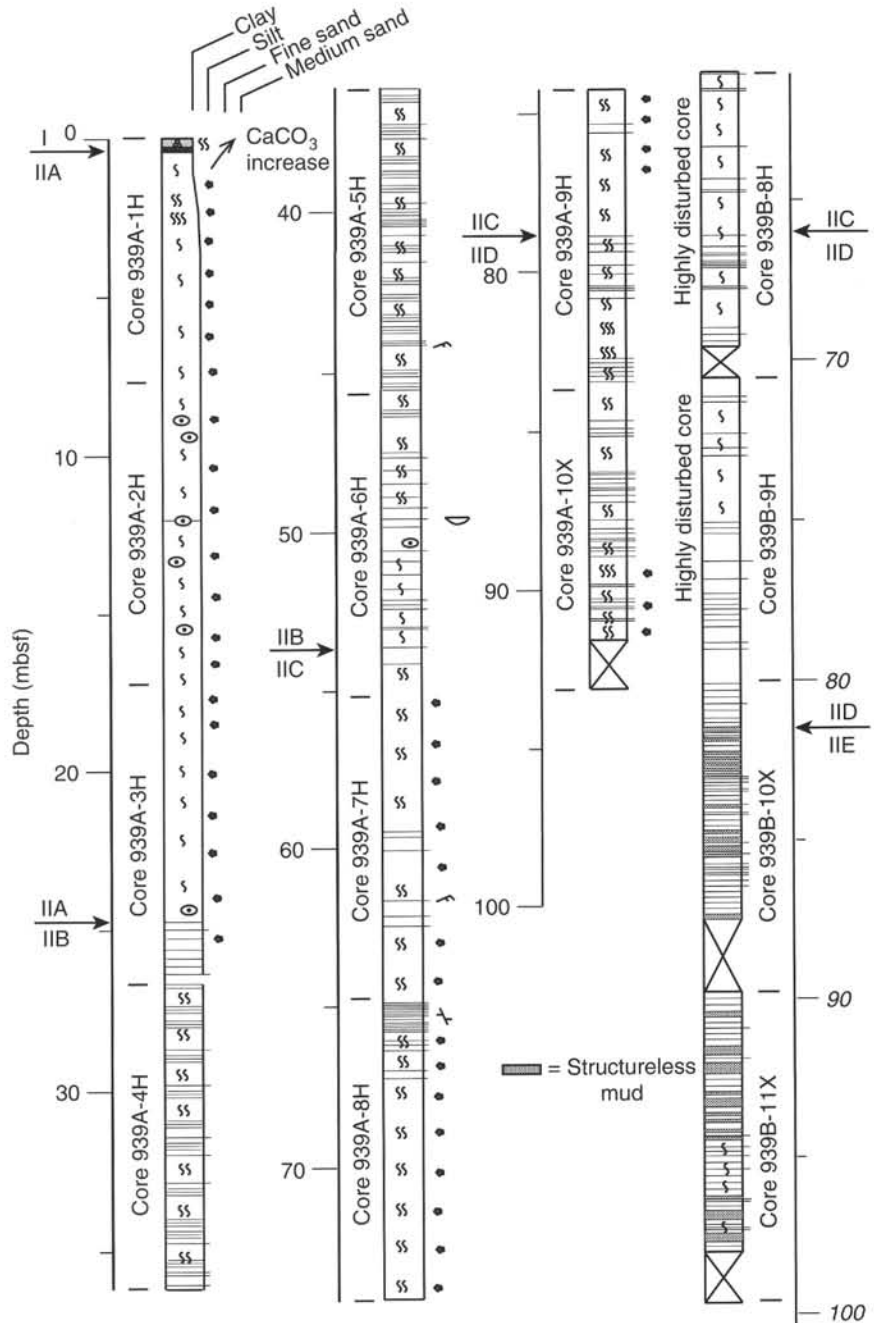
Figure 6. Graphic sedimentological columns for Site 939 showing grain-size variation (width of columns), bed thickness, and sedimentary structures; symbols and preparation of these columns are explained in the "Lithostratigraphy" section of the "Explanatory Notes" chapter, this volume. Arrows indicate the positions of unit and subunit boundaries. Hole 939A is used as the basis for the columns to the base of Subunit IID. Cores 155-939B-8H through -11X are plotted using their own depth scale (italic numbers) based on an offset of 12.6 m between the top of Subunit IID in Holes 939A and 939B (see text). The upper part of the column is shown in the strike section of the foldout (back pocket, this volume) for comparison of levee sequences on the middle and upper fan, and in the longitudinal profile of the foldout to show the down-fan changes in levee deposits.

Two lithostratigraphic units are recognized at Site 939. Units I and II are distinguished on the basis of their carbonate content and texture. Unit II is divided into five subunits, based on texture, sedimentary structures, and the scale of interbedding between silt and silty clay.

Description of Lithostratigraphic Units

Unit I

Intervals: 155-939A-1H-1, 0–68 cm; 155-939B-1H-1, 0–68 cm; 155-939C-1H-1, 0–60 cm
Age: Holocene
Depth: 0.00–0.68 mbsf

The upper part of Unit I consists of a burrowed, brown (10YR 5/3) to grayish brown (2.5Y 5/2), foraminifer-nannofossil clay (0.00 to 0.32 mbsf in Hole 939A; 0.00 to 0.38 cm in Hole 939B; 0.00 to 0.20 mbsf and disturbed in Hole 939C). This sediment is underlain in all holes by a dark reddish-brown (5YR 2.5/2) iron-rich crust, about 0.5 cm thick. Similar diagenetic crusts were analyzed previously and correlated throughout the Amazon Fan and adjacent Guiana Basin (Damuth, 1977; see "Introduction" chapter, this volume). The iron-rich crust is underlain by gray (5Y 5/1) nannofossil-rich clay. The base of Unit I is placed at a color change to dark gray (5Y 4/1), which is associated with a decrease in carbonate content. The carbonate content of Unit I decreases sharply below the iron-rich crust, and is 3.6% near the base of Unit I (see "Organic Geochemistry" section, this chapter).

Unit II

Intervals: 155-939A-1H-1, 68 cm, through -11X-CC (bottom of hole); 155-939B-1H-1, 68 cm, through -11X-CC (bottom of hole); 155-939C-1H-1, 60 cm, through -4H-CC (bottom of hole)
Age: (?)Holocene to late Pleistocene
Depth: 0.68–102.70 mbsf

Unit II consists predominantly of terrigenous clay and silty clay of dark gray (5Y 4/1) to very dark gray (5Y 3/1) color. Because color does not vary significantly throughout the unit, subunit descriptions do not refer to color. The carbonate content is less than 3.0%. Most of the sediment in this unit is stained to varying degrees by diagenetic hydrotroilite, which imparts an ephemeral black color (N2/0) to the sediment as irregular patches and/or color bands (see "Introduction" chapter, this volume). Black, soft hydrotroilite micronodules (1–2 mm diameter) are common. Larger hydrotroilite concretions and continuous bands are present from 8 to 16 mbsf at all holes (e.g., Fig. 6).

Unit II is divided into five subunits based mainly on the frequency of silt laminae and beds (Figs. 5 and 6).

Subunit IIA

Subunit IIA extends from the base of Unit I to 24.45 mbsf in Hole 939A (from Section 939A-1H-1 at 68 cm through -3H-7 at 30 cm) and 23.00 mbsf in Hole 939B (from Section 939B-1H-1 at 68 cm through -3H-CC). The sediment consists almost entirely of either clay or silty clay with intense to slight bioturbation and scattered hydrotroilite nodules and bands. The base of the subunit is placed at the top of the first silt lamina in Unit II.

Subunit IIB

Subunit IIB extends from 24.45 to 54.48 mbsf in Hole 939A (from Section 939A-3H-7 at 30 cm through -6H-7 at 75 cm) and 23.00 to 44.23 mbsf in Hole 939B (Section 939B-4H-1 through -6H-3 at 52 cm). The sediment is moderately burrowed and/or color-banded silty clay (Fig. 7) with thin laminae and beds of silt. Some of the apparent color-banding may result from burrows parallel to bedding. In Subunit IIB at Hole 939A, there are 25 silt laminae and nine silt beds all less than 3 cm thick. In Hole 939B, where this subunit is 30% thinner, there are 19 silt laminae and five silt beds all less than 3 cm thick.

Silt layers commonly have sharp bases and gradational tops. Many are parallel laminated or wavy laminated (Fig. 8); only a few have a cross-laminated basal division. Some layers pass upward into laminated mud that does not contain the hydrotroilite micronodules that characterize the burrowed sediment (Fig. 9). Burrows cut and destroy the primary lamination in parts of some silt layers, and in other cases silt-enriched burrows suggest complete bioturbation of a silt turbidite.

A thin section of color-banded silty clay in Subunit IIB (Sample 939A-4H-3, 146–150 cm) contains micronodules of both hydrotroilite and vivianite. The hydrotroilite micronodules fill porosity in the sediment, have diffuse margins, and locally form lenses parallel to bedding (Fig. 10A). The vivianite micronodules displace surrounding sediment, have sharp margins, and are equant. Growth of vivianite micronodules locally deforms hydrotroilite bands, suggesting that the hydrotroilite formed first (Fig. 10B).

Subunit IIC

Subunit IIC extends from 54.48 to 78.73 mbsf in Hole 939A (from Section 939A-6H-7 at 75 cm through -9H-4 at 10 cm) and 44.23 to 66.17 mbsf in Hole 939B (from Section 939B-6H-3 at 50 cm through -8H-5 at 122 cm). The sediment is mainly moderately burrowed silty clay (Fig. 6) with the exception of a short interval of color-banded and slightly burrowed silty clay that alternates with numerous laminae and beds of silt (Fig. 11). This coarser grained interval is 2.42 m thick in Hole 939A and 1.65 m thick in Hole 939B (Section 939A-8H-1 at 15 cm through -8H-2 at 135 cm; Section 939B-7H-3 at 17 cm
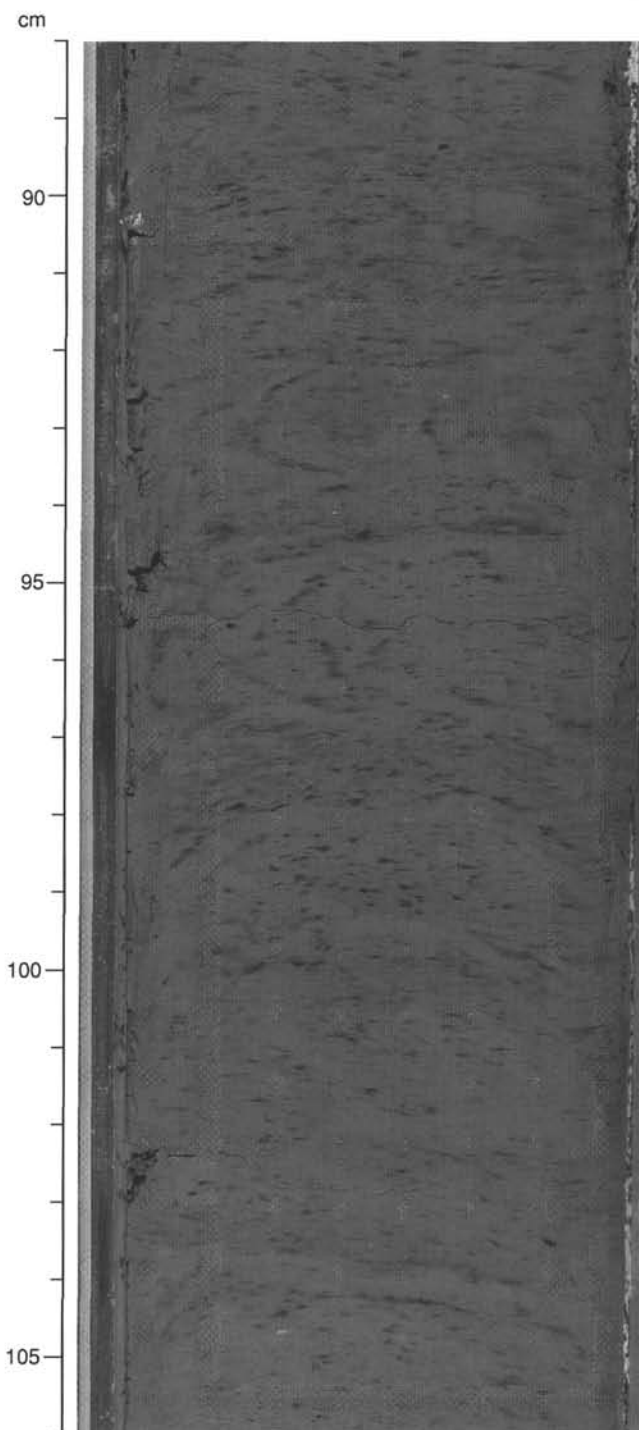
Figure 7. Spreiten-filled burrows (?*Echinocardium*), each about 1–2 cm from top to bottom, in Subunit IIB. Burrow margins are marked by light-colored pseudolaminae that are free of black hydrotroilite stain (interval 155-939A-4H-3, 88–106 cm).

through -7H-4 at 67 cm). In Hole 939A, the 2.42-m-thick interval contains 18 laminae and six beds of silt, all thinner than 3 cm. In Hole 939B, the equivalent 1.65-m-thick interval contains 23 silt laminae and no silt beds. A normal fault with an apparent dip of 70° displaces some of the silt beds in this interval by about 1 cm at Hole 939A (Fig. 12).

cm
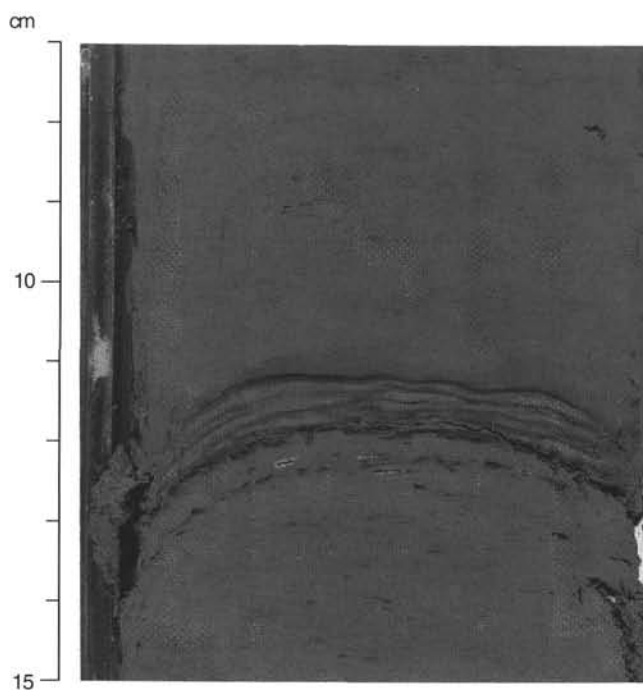
Figure 8. Sharp-based silt lamina in Subunit IIB, with its internal wavy lamination denoted by black, hydrotroilite staining (interval 155-939A-4H-7, 7–15 cm).

Subunit IID

Subunit IID extends from 78.73 mbsf to the bottom of Hole 939A (from Section 939A-9H-4 at 10 cm through -11X-CC) and 66.17 to 81.50 mbsf in Hole 939B (from Section 939B-8H-5 at 122 cm through -10X-2 at 0 cm). This subunit resembles Subunit IIB, except for a greater concentration of silt laminae and beds (Fig. 6). In Hole 939A, there are 42 silt laminae, nine silt beds less than 3 cm thick, and one 5-cm-thick silt bed. In Hole 939B, where this subunit is 30% thinner, there are 17 silt laminae, five silt beds all less than 3 cm thick, and one 3-cm-thick very fine sand bed. Subunit IID appears to contain fewer silt layers per unit thickness in Hole 939B, but both Cores 939B-8H and -9H have highly disturbed sections, and some silt-rich intervals may not have been recovered.

Subunit IIE

Subunit IIE occurs only in Hole 939B, from 81.50 mbsf to the bottom of the hole at 99.4 mbsf (Section 939B-10X-2 through -11X-CC). The top of the subunit is placed at the top of the first bed of structureless silty clay that characterizes Subunit IIE. About half of the sediment in this subunit is color-banded silty clay with 18 silt laminae and 11 silt beds all thinner than 3 cm. The remainder consists of beds, 5 to 30 cm thick, of silty clay that contain no obvious lamination or burrows (Fig. 13).

Mineralogy

Fine-fraction mineralogy was determined by X-ray-diffraction analysis of 10 bulk samples of silty clay. The common minerals in these samples are quartz, plagioclase, augite, and the clay minerals smectite, illite (+ mica), and kaolinite (Table 3). A few samples contain K-feldspar and amphibole (probably hornblende based on examination of a few smear slides). Relative to quartz, the abundances of feldspars and ferromagnesian minerals show little stratigraphic variation (Fig. 14A).

The phyllosilicate mineral group with the highest relative peak intensity is illite + mica (Fig. 14B). Total clay minerals (+ mica) in-

cm
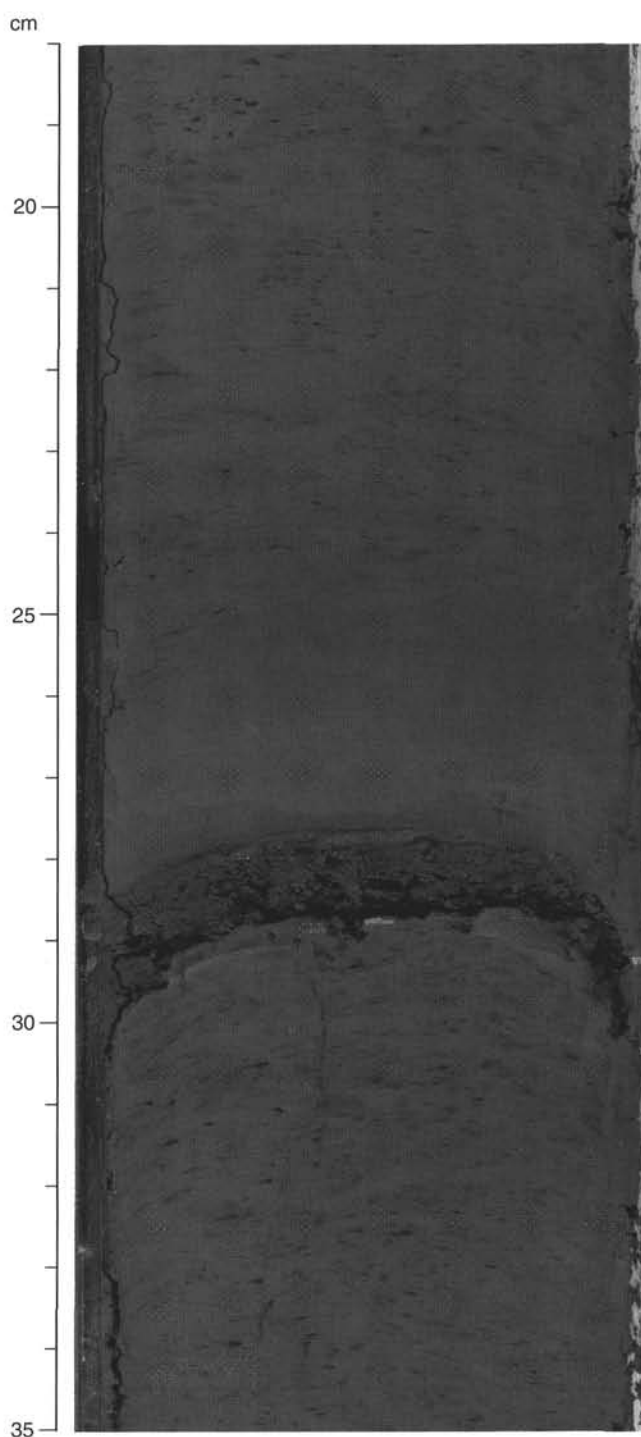
Figure 9. Sharp-based silt lamina in Subunit IIB, overlain (with distinct gradation) by a light-colored, subtly laminated mud cap between scale divisions 25 and 28 cm. The surrounding burrowed sediment contains disseminated, soft, hydrotroilite micronodules (interval 155-939A-4H-4, 18–35 cm).

crease from 30 to 50 mbsf, across the boundary between Subunits IIB and IIC (Fig. 14A).

Spectrophotometry

In Unit II, reflectance values are 15%–27% for all wavelength bands from 400 to 700 nm. Correlations between reflectance values
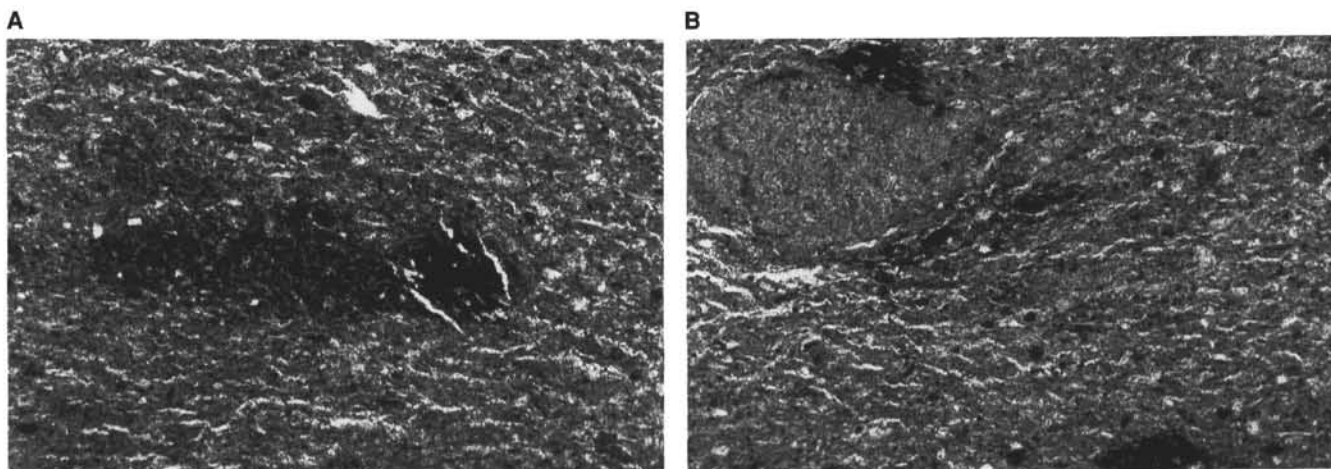
Figure 10. Photomicrographs of diagenetic micronodules in plane-polarized light (Sample 155-939A-4H-3, 146–150 cm). **A.** A 0.15-mm-diameter black hydrotroilite micronodule that passes laterally into more weakly stained silty clay. **B.** An equant, 0.33-mm-diameter vivianite micronodule (upper left corner), which bows primary layering in the surrounding hydrotroilite-stained silty clay. Scale for (A) and (B): 0.5 mm = 55 mm on photo.

and lithostratigraphic subunits of Unit II are not apparent. The highest reflectance values (30%) are in the calcareous clay of Unit I.

There is a weak correspondence in Hole 939B between the ratio of red (650–700 nm) and blue (450–500 nm) spectral reflectance (Fig. 5) and the occurrence of iron as oxidized or reduced phases. In particular, positive deviations from the mean red/blue reflectance value of 1.14 are associated with a high content of iron oxyhydroxides in Unit I, and the most negative deviations at 8 to 24 mbsf, in muds of Unit II, are attributed to abundant hydrotroilite.

Discussion

The three holes at Site 939 all penetrate the eastern levee of the Amazon Channel: Hole 939A is about 1000 m east of the levee crest, and Holes 939B and 939C are about 480 m farther east. The levee sediment is generally fine-grained mud, except for concentrations of silt laminae and beds in Subunits IIB, middle of IIC, and IID. The recovered sediment provides little insight into the origin of the stratal discontinuity at about 15 mbsf seen in the 3.5-kHz profile over the site (see "Setting and Objectives" section, this chapter). The only features at this depth are common 1- to 2-cm-sized hydrotroilite nodules and some approximately horizontal hydrotroilite layers.

On a scale of a few tens of meters vertically, asymmetric cycles in the frequency or thickness of silt layers are not apparent within Unit II. Instead, the silt layers tend to occur in "clusters" or "packets" (Fig. 6). On a larger scale, there is an overall fining upward from Subunit IIB into Subunit IIA and into the hemipelagic Unit I. This fining is attributed to a progressive reduction in sediment supply to the Amazon Fan during the latest post-glacial sea-level rise.

Structureless mud beds are found only in Subunit IIE. These might be mud turbidites or the deposits of thin mud flows.

There is a pronounced thinning of the entire stratigraphic section from Hole 939A, which is closer to the Amazon Channel, to Hole 939B. This thinning is consistent with the interpretation of 3.5-kHz reflection profiles at the site (Figs. 2, 3, 4). All units except Unit I show this thinning, verifying that Unit I is the most pelagic of the lithostratigraphic units, thus forming a drape of uniform thickness. Both the number and thickness of silt laminae and beds decrease away from the channel; this decrease might indicate that the silt layers are lenticular on a lateral scale of tens to hundreds of meters, perhaps because the turbidity currents deposited progressively less sediment as they accelerated down the backslope of the levee.

BIOSTRATIGRAPHY

Calcareous Nannofossils

Calcareous nannofossils recovered at Site 939 are all from Zone CN15b (Table 4). An abundant, well-preserved, and diverse nannofossil assemblage is present in the calcareous nannofossil and foraminifer clay in the mud-line sample, and includes species of dissolution-prone genera such as *Scyphosphaera* and *Pontosphaera*. Nannofossils are absent or occur in low abundance in Unit II in Holes 939A and 939B (Samples 939A-1H-CC, 17–18 cm, through -11X-CC, 22–23 cm, and 939B-1H-CC, 52–53 cm, through -11X-CC, 9–10 cm). All assemblages have a low diversity and are affected by dissolution. Only dissolution-resistant species like *G. oceanica* and *C. leptoporus* are present. Subunit IIC and the upper part of Subunit IID are barren of calcareous nannofossils, which may be a result of dissolution coupled with a higher sedimentation rate during deposition of these subunits. The occurrence of *E. huxleyi* places the glacial-age sediment of Unit II in Zone CN15b.

Planktonic Foraminifers

The boundary between Ericson Zones Z and Y (disappearance of *G. tumida*) is placed between Samples 939B-1H-CC, 82–84 cm (0.82 mbsf), and -1H-1, 130–134 cm (1.30 mbsf; Fig. 15; Table 5). The occurrence of *G. tumida* in core catchers lower in the hole is most likely the result of downhole contamination. Foraminifers are common to abundant in Unit I and Subunit IIA from 0 to 4 mbsf (Samples 939B-1H-1, 27–29 cm, through -1H-CC, 5–14 cm). The interval between the Z/Y boundary and 97.86 mbsf (Sample 939B-11X-CC, 0–9 cm), which corresponds to Subunits IIB through IIE (Fig. 15), has been defined as the Y Zone on the basis of the absence of *G. menardii* and *G. tumida*. This interval can also be constrained in age to less than 40 ka by the absence of *P. obliquiloculata*.

Foraminifer abundances are low from 13.4 mbsf (Sample 939B-2H-CC, 43–52 cm) to the bottom of the hole at 97.86 mbsf (Sample 939B-11X-CC, 0–9 cm). Unit I and Subunit IIA contain pteropods. Unit I and Subunits IIA, IIB, and IIC contain high abundances of authigenic minerals consisting of red and black nodules (Samples 939B-1H-1, 27–29 cm [3.9 mbsf], through -7H-CC, 45–54 cm [62 mbsf]). Mica also occurs in the lower portion of Subunit IIC from 68.98 mbsf (Sample 939B-8H-CC, 54–63 cm) to the bottom of the hole. Iron-stained foraminifers occur from 23.9 to 33.12 mbsf (Sam-
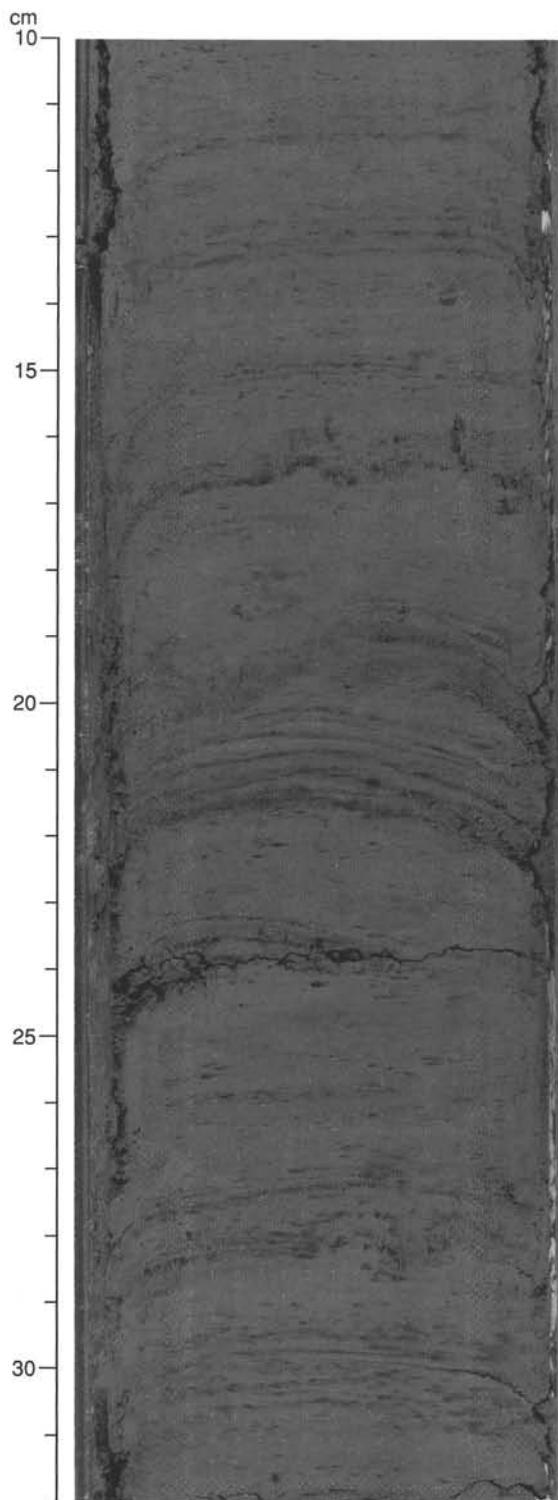
Figure 11. Color banding and silt laminae (e.g., at scale divisions 21–22 cm) in the central part of Subunit IIC (interval 155-939A-8H-1, 10–32 cm).

Figure 12. Normal offset of silt laminae by a steep fault in the middle of Subunit IIC. Offset of a pair of laminae is clearest between scale divisions 53 and 55 cm (interval 155-939A-8H-1, 45–65 cm).

ples 939B-3H-CC, 5–14 cm, through -4H-CC, 14–23 cm) in Subunit IIB and at 80.4 mbsf (Sample 939B-9H-CC, 47–56 cm) in Subunit IID. Echinoid spines are found in the lower portions of the hole from 23.92 to 80.4 mbsf (Samples 939B-3H-CC, 5–14 cm, through -9H-CC, 47–56 cm).

Benthic Foraminifers

In the entire hole, benthic foraminifers are rare or absent. In Subunits IIA and IIC, abyssal benthic foraminifers occur in low abundances (Samples 939B-1H-1, 130–134 cm [1.34 mbsf], and 939B-6H-CC, 33–42 cm [52.28 mbsf]). Bathyal benthic foraminifers are absent in Hole 939B.

cm

95 —

100 —

105 —

110 —
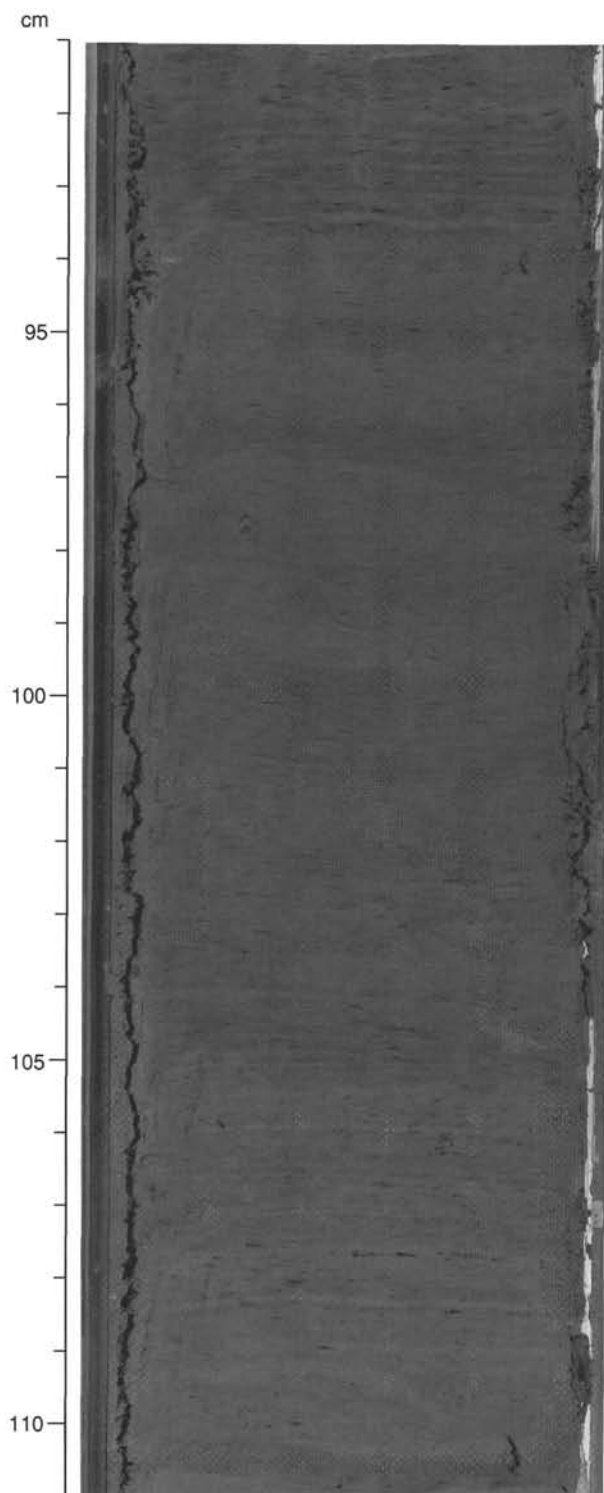
Figure 13. Example of a bed of structureless mud, between scale divisions 94 and 104 cm. Very subtle horizontal banding in this interval is caused by cleaning of the core surface with a spatula, not by internal laminations. The surrounding sediment is color-banded silty clay. There is a 1-cm-high burrow at scale division 110 cm (interval 155-939B-10X-2, 91–111 cm).

Siliceous Microfossils

Site 939 is barren of diatoms, except in the mud-line sample where both marine and freshwater diatoms occur in low abundance (e.g., *Actinocyclus curvatulus* and *Melosira granulata*; Table 5). Siliceous sponge spicules are present in Holes 939A, 939B, and 939C in Unit I, Subunit IIA, and the lower parts of Subunits IID and IIE (Table 4).

Palynology

Four samples from Unit II were examined from Hole 939A (Table 6) and contained low abundances of pollen and spores with moderate to poor preservation. Present in the assemblages were Compositae, tricolporate (TCP) and triporate (TP), Euphorbiaceae and monosulcus (probably Palmae) pollen types, and monolete spores. Dinoflagellates were not found. Wood particles were observed in moderate abundance in all samples.

Stratigraphic Summary

Calcareous nannofossils and planktonic foraminifers indicate that the age of the sediment at Site 939 covered an interval from Holocene to late Pleistocene. Palynomorphs have low abundance at this site. Unit I contains nannofossil and planktonic foraminifer assemblages indicative of the Holocene. The nannofossil assemblages are well preserved and represent nannofossil Zone CN15b. The Z/Y boundary was not precisely defined on the ship, but is most likely near the base of Unit I (Fig. 15). Previous sites indicate that the Z/Y boundary occurs below the iron-rich crust. Planktonic foraminifers are found in low abundance, and nannofossils are absent in Subunits IIB and IIC. All of Unit II below the Z/Y boundary has been defined as the Y Zone on the basis of the absence of *G. menardii* and *G. tumida*. The age of this unit can also be constrained to younger than 40 ka due to the absence of *P. obliquiloculata*.

PALEOMAGNETISM

Remanence Studies

Archive-half sections from all 22 APC and four XCB cores were measured on the pass-through cryogenic magnetometer system. Cores 939A-3H through -9H and Cores 939B-3H through -9H were oriented with the Tensor tool, which performed flawlessly. Only Cores 939A-8H and -9H showed progressive westward drift (~40°) of declination, or twisting downward, within each core.

A 40-m interval of Hole 939A (20 to 60 mbsf in Fig. 16) displayed three well-defined oscillations in declination over a range of ~80°. Inclination data from Holes 939A, 939B, and 939C for 0–35 mbsf are shown in Figure 17. The least noisy data set appears in Hole 939A, where oscillations in inclination suggest two wavelengths. The longer wavelength is seen as two cycles with lengths of 8 to 20 m, respectively, and with an amplitude of ~45°. Tie points that define these cycles occur at 5, 13, and 32 mbsf in Hole 939A; 3, 11, and 29 mbsf in Hole 939B; and 3.5, 12.5, and 32 mbsf in Hole 939C. The shorter wavelength consists of numerous cycles ~1.75 m in length, and with an amplitude of 5° to 15°. After AF demagnetization to 20 mT, remanence intensity oscillations also display two characteristic wavelengths (Fig. 18). A shorter wavelength (~1 m) cycle is observed in Hole 939A from 0 to 20 mbsf. Longer wavelength (20 to 40 m) cycles are apparent in the Hole 939B record from 0 to 100 mbsf.

If the declination swings from 20 to 60 mbsf in Figure 16 represent a 1500-yr secular variation cycle, the 40-m interval would represent ~4500 yr, with a sedimentation rate of ~9,000 m/m.y. An average sedimentation rate of ~9,000 m/m.y. would also be indicated for the interval plotted in Figure 17, if the long period declination cy-

Table 3. Relative peak intensities of the main minerals in silty clay samples from Hole 939B.

Core, section, interval (cm)	Depth (mbsf)	Relative intensity of primary peaks							
		Smectite	Mica + Illite	Kaolinite	Quartz	Plagioclase	K-feldspar	Augite	Hornblende
155-939B-									
1H-2, 92–93	2.42	9.4	10.6	5.0	100.0	7.2	*	2.7	*
2H-4, 50–51	9.00	5.8	13.9	8.6	100.0	7.1	4.1	2.1	*
3H-5, 74–75	19.08	7.1	15.4	8.6	100.0	7.6	*	2.2	*
4H-4, 40–41	27.90	7.2	15.9	7.9	100.0	7.5	*	2.2	*
6H-6, 69–70	48.90	11.2	21.0	9.7	100.0	9.7	*	3.1	*
7H-6, 68–69	58.35	12.4	21.7	13.9	100.0	10.6	*	3.2	*
8H-5, 69–70	65.64	8.9	24.7	12.3	100.0	7.8	*	2.9	1.5
9H-5, 69–70	76.25	7.5	21.1	10.0	100.0	8.7	*	3.3	3.2
10X-5, 68–69	86.68	3.6	17.2	10.3	100.0	8.3	*	2.0	*
11X-2, 69–70	91.89	11.8	24.2	12.0	100.0	8.7	4.7	2.3	*

Notes: See "Lithostratigraphy" section in the "Explanatory Notes" chapter, this volume, for XRD methods. * = non-detection.
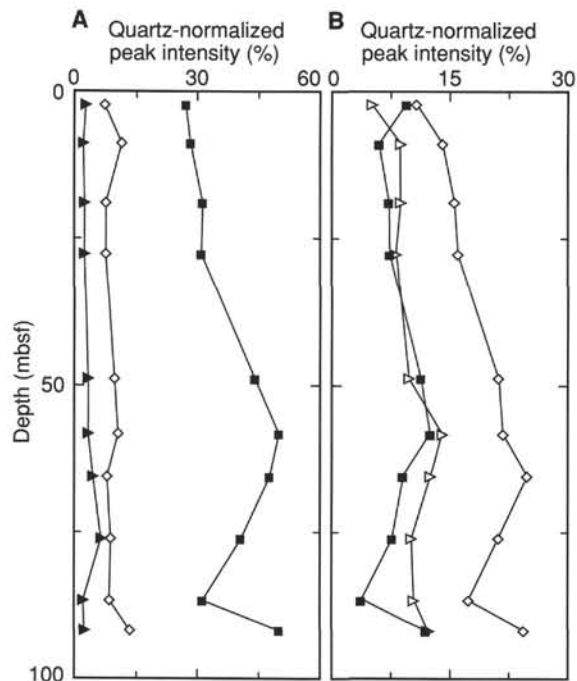
Figure 14. Relative abundances of silicate minerals in silty clay samples, based on XRD analysis (Table 3). **A.** Plot against depth of the quartz-normalized peak intensities of the major mineral groups (quartz peak intensity set at 100%). Squares = clay minerals + mica; diamonds = feldspar; triangles = augite + hornblende. **B.** Plot against depth of the quartz-normalized peak intensities of clay minerals and micas. Squares = smectite; diamonds = illite (+ mica); triangles = kaolinite.

cles again represent 1500 yr. The shorter period inclination and remanence intensity cycles would then correspond to periods of ~100–200 years. Although some part of the long wavelength oscillations in remanence intensity may relate to fluctuations in the strength of the geomagnetic field, they may also arise from changes in the remanence-carrying ability of the sediment. Post-cruise magnetic analyses of the sediment should allow us to separate these two variables to give a record of long period changes in geomagnetic field intensity.

Magnetic Susceptibility Studies

Whole-core magnetic susceptibility was measured on all cores from this site. Discrete sample measurements were performed only for Hole 939B (Fig. 19). Uniformly high whole-core susceptibility values are found within Subunit IIA, and the lowest values are within

Unit I. In general, there is no apparent correlation between the location of unit/subunit boundaries and the susceptibility record.

A possible correlation scheme between Holes 939A and 939B is given in Figure 20 based on correlations in remanence inclination (Fig. 17). The susceptibility data were smoothed using a five-point moving average. The tie points were constrained by the locations of the Unit II subunit boundaries (see "Lithostratigraphy" section, this chapter). The correlations indicate that the depths of the tie points have a relatively constant offset between the two holes with a slope of 0.871 ($r^2 = 0.99$).

ORGANIC GEOCHEMISTRY

Volatile Hydrocarbons

Gas analyses were performed in samples from Hole 939A down to 86.70 mbsf. Headspace methane concentrations increase rapidly below the sediment surface to a maximum value of 33,270 ppm at 16.70 mbsf (Table 7; Fig. 21). Methane concentrations remain fairly constant below this depth, ranging from 6,600 ppm to 15,000 ppm. Vacutainer methane values are considerably higher than headspace concentrations (Fig. 21), ranging from 74,000 ppm at 17.41 mbsf to 539,510 ppm at 77.13 mbsf. Higher molecular weight hydrocarbons were not measured, indicating a predominantly biogenic methane source at Site 939.

Carbon, Nitrogen, and Sulfur Concentrations

Elemental analyses were performed on samples from Hole 939B down to 93.18 mbsf and on Hole 939C to 36.00 mbsf. Every section from Hole 939C was sampled as part of a high-resolution study of the top 40 mbsf. The data from both holes are presented together, and the high-resolution samples are discussed separately at the end of this section.

In both Holes 939B and 939C, calculated $CaCO_3$ contents range from 0.5% to 3.6% (Table 8; Fig. 22). The highest value (3.6%) is found at 0.50 mbsf, near the bottom of the carbonate-rich Unit I (see "Lithostratigraphy" section, this chapter). TOC concentrations range from 0.5% to 1.0%, and most of the low values (<0.8%) are from the top 2 mbsf. Total nitrogen concentrations range between 0.04% and 0.12%. The lowest TN concentrations (<0.07%) are measured in the top 8.09 mbsf of Hole 939C. Total sulfur is low (<0.3%) throughout Site 939. The only exception is the sample at 30.66 mbsf in Hole 939B, which has a TS content of 1.21%. This sample corresponds to a black-stained silt layer enriched in hydrotroilite.

High-resolution Samples from Hole 939C

One of the major objectives of Hole 939C was to investigate the factors that control vivianite precipitation, which is thought to occur

Table 4. Calcareous nannofossil and siliceous microfossil abundance data for Holes 939A, 939B, and 939C.

Core, section, interval (cm)	Top interval (mbsf)	Bottom interval (mbsf)	Calcareous nannofossils		Diatoms		Sponge spicules	Radiolarians	Ericson zone (inferred from foraminifers)	Age (inferred from foraminifers)
			Abundance	Zone	Marine	Freshwater				
155-939A-										
1H-CC, 17–18	7.67	7.68	r	CN15b	vr	b	f	b	Z	late Pleist.
2H-CC, 32–33	17.62	17.63	vr		b	b	b	b	Y	late Pleist.
3H-CC, 39–40	26.37	26.38	tr		b	b	b	b	Y	late Pleist.
4H-CC, 24–25	36.77	36.78	b		b	b	b	b	Y	late Pleist.
5H-CC, 113–114	45.73	45.74	b		b	b	b	b	Y	late Pleist.
6H-CC, 123–124	56.85	56.86	b		b	b	f	b	Y	late Pleist.
7H-CC, 75–76	65.01	65.02	b		b	b	b	b	Y	late Pleist.
8H-CC, 14–15	74.26	74.27	tr		b	b	b	b	Y	late Pleist.
9H-CC, 25–26	84.04	84.05	b		b	b	r	b	Y	late Pleist.
10X-CC, 20–21	91.54	91.55	vr		b	b	vr	b	Y	late Pleist.
11X-CC, 22–23	96.21	96.22	vr		b	b	b	b	Y	late Pleist.
155-939B-										
1H-M1, 0	0.00	0.00	a	CN15b	vr	b	c	b	Z	Holocene
1H-1, 0–1	0.00	0.01	a		b	b	a	b	Z	Holocene
2H-CC, 52–53	13.42	13.43	b		b	b	b	b	Y	late Pleist.
3H-CC, 14–15	23.92	23.93	b		b	b	b	b	Y	late Pleist.
4H-CC, 23–24	33.12	33.13	b		b	b	b	b	Y	late Pleist.
5H-CC, 72–73	43.07	43.08	tr		b	b	b	b	Y	late Pleist.
6H-CC, 42–43	52.28	52.29	b		b	b	b	b	Y	late Pleist.
7H-CC, 54–55	62.00	62.01	vr		b	b	b	b	Y	late Pleist.
8H-CC, 63–64	68.98	68.99	tr		b	b	vr	b	Y	late Pleist.
9H-CC, 56–57	80.42	80.43	vr		b	b	b	b	Y	late Pleist.
10X-CC, 9–10	87.49	87.50	vr		b	b	vr	b	Y	late Pleist.
11X-CC, 9–10	97.86	97.87	vr		b	b	r	b	Y	late Pleist.
155-939C-										
1H-M1, 0		0.00	a	CN15b	b	b	f	b	Z	Holocene
1H-1, 0–1	0.00	0.01	a		b	b	a	b	Z	Holocene
1H-CC, 13–14	7.59	7.60	vr		b	b	b	b	Z	late Pleist.
2H-CC, 34–35	17.64	17.65	tr		b	b	b	b	Y	late Pleist.
3H-CC, 44–45	26.09	26.10	tr		b	b	b	b	Y	late Pleist.
4H-CC, 56–57	36.92	36.93	b		b	b	b	b	Y	late Pleist.

in the top 20 mbsf. We analyzed the elemental composition of the samples from each section in Hole 939C to characterize organic matter degradation over this interval.

The elemental data at Site 939 indicate an overall similar organic matter composition (Fig. 22). However, slight changes in elemental compositions over the top 30 m could be related to diagenetic changes observed in the pore waters. For example, the relatively low TN values (<0.07%) measured between 0.5 and 8.0 mbsf in Hole 939C (Fig. 22) could be indicative of preferential oxidation of reactive nitrogenous organic compounds. Because the TN concentrations are so low, however, it is difficult to ascertain whether these differences are significant. Additional analyses of more reactive organic fractions, such as lipids or amino acids, will be necessary to assess the effect of organic matter diagenesis on pore-water chemistry and vivianite formation.

INORGANIC GEOCHEMISTRY

Interstitial Water Analysis

Interstitial waters were collected from 28 sediment samples at Site 939, eight from Hole 939B and 20 from Hole 939C. For Hole 939B, samples were taken approximately one every 10 m for the upper 40 mbsf and approximately one every 30 m thereafter to a depth of 97.10 mbsf (Table 9; Fig. 23). For Hole 939C, a high-resolution suite of samples was taken with sample intervals of approximately 1.5 m for the first 18.50 mbsf, and 3 m thereafter to 37.00 mbsf. In general, the trends observed in the two holes are very similar. There are, however, some small offsets from one hole to the other in the observed depths of particular features, for example, the peak in alkalinity or phosphate concentration. In all cases where there are differences, the depths in Hole 939B are greater. Lithostratigraphic correlation between the two holes shows that below 20 mbsf, features in Hole 939C are found approximately 1 m shallower than in Hole 939B. Thus, part of the offset must reflect slightly different geochemical gradients between the two sites.

Salinities of the water samples range from 32.5 to 35.0 (Fig. 23A). For both holes, the salinity decreases steadily from a near-surface value of 35 to 32 downhole. The salinity reaches 32.5 at 59.07 mbsf in Hole 939B, and at 28.00 mbsf in Hole 939C.

Chloride concentrations increase with depth throughout the holes (Fig. 23B). The near-surface chloride concentration is 551 to 552 mM. The concentration increases to 558 at 37.00 mbsf, near the bottom of Hole 939C, and to 564 at 97.10 mbsf, near the bottom of Hole 939B.

Pore-water pH varies within a narrow range, from 7.55 to 7.76, in Hole 939C and tends to increase downhole (Fig. 23C). The downhole increase could be an artifact of increased time between sampling and analysis for deeper samples, which would allow more time for CO_2 degassing. In Hole 939B, pH decreases slightly downhole, from a value of 7.71 at 1.45 mbsf to 7.46 near the bottom of the hole.

Alkalinity values increase rapidly in the upper 10 mbsf (Fig. 23D), from 4.70 mM at 0.20 mbsf to 31.56 mM at 9.00 mbsf (or 33.29 mM at 11.45 mbsf in Hole 939B). From 10 to about 40 mbsf, alkalinity decreases steadily to about 10 mM. Alkalinity remains near 10 mM throughout the remainder of the hole.

Magnesium and calcium profiles are again similar to those at previous sites. The concentrations decrease from 54.7 mM magnesium and 12.0 mM calcium at 0.20 mbsf to around 43 mM magnesium and 4 mM calcium at around 30 mbsf (Fig. 23E and 23F). Thereafter, the values are fairly constant downhole. A plot of magnesium vs. calcium concentrations for Hole 939C (Fig. 24) shows a strong correlation between the two ($r^2 = 0.96$ with a slope of 0.85). The correlation suggests that calcium and magnesium losses from the pore fluids are related to each other. One possibility is that both are precipitated as a carbonate mineral, which is supported by considering the possible sources and sinks for alkalinity as discussed below.

Pore-water sulfate concentrations are 27.0 mM at 0.20 mbsf, within analytical uncertainty of the seawater value. By 1.40 to 1.45 mbsf, however, the concentration has fallen to around 21 mM, indicating anoxia and significant sulfate reduction (Fig. 23G). Sulfate concentrations continue to decrease with depth and have fallen to
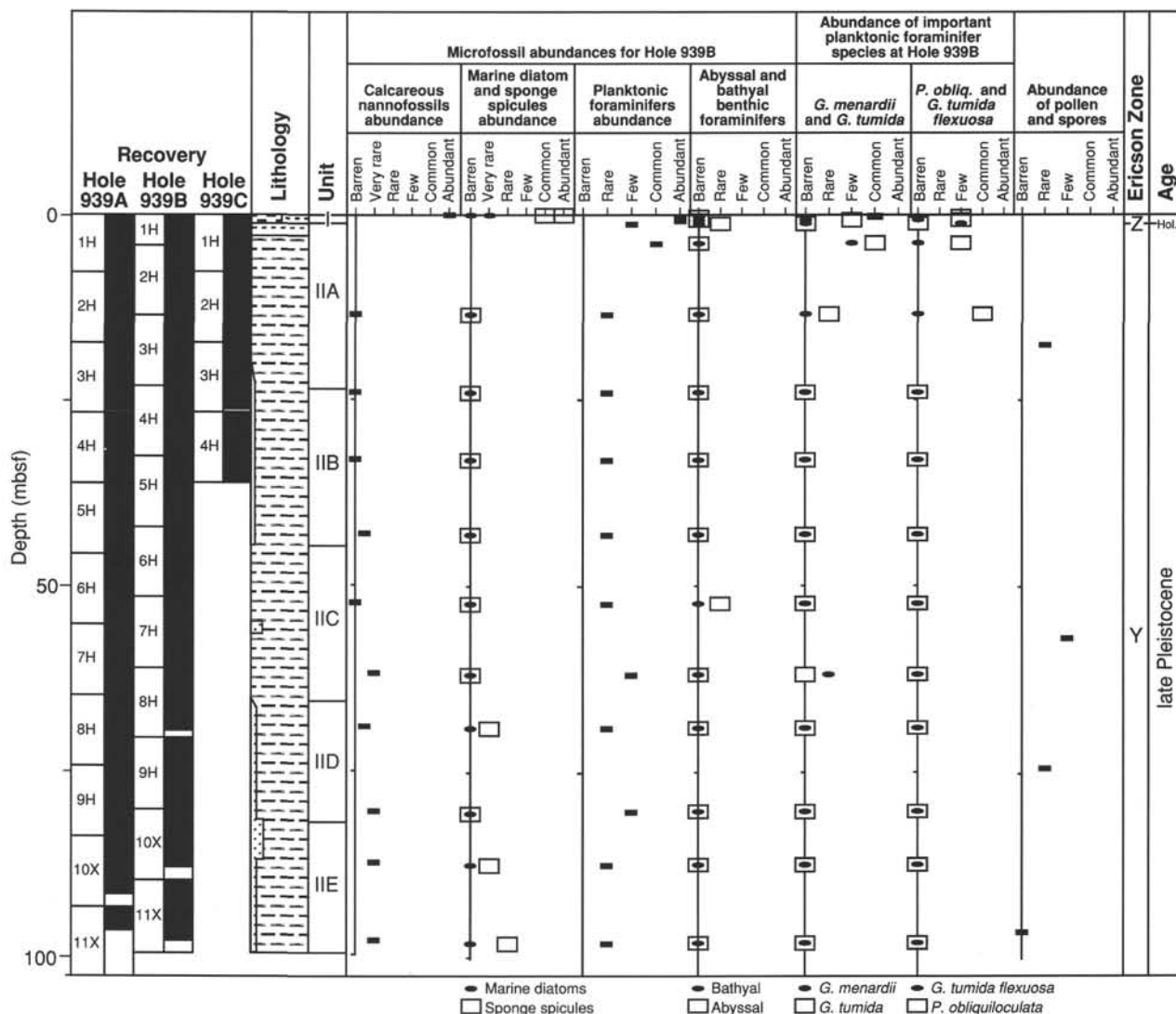
Figure 15. Biostratigraphic summary for Site 939.

zero by 9.00 mbsf. The values remain at or near zero for most of the remainder of the hole.

Sulfate reduction has been shown to produce alkalinity through organic-matter oxidation by the following overall reaction stoichiometry:

$$2CH_2O + SO_4^{2-} = 2HCO_3^- + H_2S,$$
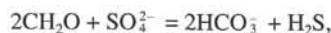
so that 2 moles of alkalinity should be produced for 1 mole of sulfate reduced. Precipitation of a carbonate mineral, on the other hand, should remove 2 moles of alkalinity for each mole of calcium or magnesium precipitated as carbonate. Summing the source (sulfate reduction) and sinks (the pore water, and calcium and magnesium removal) of alkalinity shows that the amount of alkalinity that should have been produced from sulfate reduction minus the alkalinity remaining in the pore fluids is very closely balanced by the combined losses of calcium and magnesium. This "alkalinity balance" indicates that almost all the alkalinity removed from the pore fluids can be accounted for as precipitation of calcium or magnesium carbonate.

Ammonium concentrations increase with depth over the entire depth range of both holes (Fig. 23H). The increase is initially rapid, from 0.1 mM at 0.20 mbsf to 5.1 mM at 16.50 mbsf. Thereafter, the

concentrations increase more slowly with depth, to around 7.2 mM at 97.10 mbsf.

Pore-water phosphate concentrations exhibit a distinct sub-bottom maximum at around 10 mbsf (Fig. 23I). The concentrations are around 30 µM near the sediment surface, and increase to 97.7 µM by 11.45 and 9.00 mbsf in Holes 939B and 939C, respectively. As at Site 931, the peak in phosphate concentration is coincident with the depth of complete sulfate reduction, suggesting that vivianite precipitation takes place primarily below the zone of sulfate reduction. From around 10 to 30 mbsf, the phosphate concentration decreases, falling to less than 10 µM. Several small peaks in phosphate concentration appear in the higher resolution record from Hole 939C over this interval. Below 30 mbsf, phosphate concentration remains below 10 µM.

Dissolved silica concentrations show much more variability in Hole 939C than in Hole 939B. In Hole 939B, the concentrations increase from 303 µM at 1.45 mbsf to 405 µM at 11.45 mbsf, and remain near 400 µM downhole. Concentrations in the upper part of Hole 939C also increase, from 256 µM to around 400 µM at 7.40 mbsf. However, two sharp local minima, of below 200 µM, occur at 16.50 and 34.00 to 37.00 mbsf (Fig. 23J).

Pore-water potassium concentrations decrease from 13 mM near the sediment surface to about 9 mM at 30 mbsf (Fig. 23K). Below 30

Table 5. Foraminifer abundance data for Hole 939B.

Core, section, interval (cm)	Top interval (mbsf)	Bottom interval (mbsf)	Globorotalia menardii	Globorotalia tumida	Globorotalia tumida flexuosa	Pulleniatina obliquiloculata	Globigerinoides ruber (white)	Globigerinoides ruber (pink)	Globorotalia hexagonus	Neogloboquadrina dutertrei	Globigerinoides trilobus trilobus	Globorotalia inflata	Globorotalia truncatulinoides	Globigerina bulloides	Globigerinoides trilobus sacculifer	Globorotalia fimbriata	Bolliella adamsi	Hastigerinella digitata	Globigerina calida calida	Globorotalia crassaformis hessi	Globorotalia crassaformis viola	Globorotalia tosaensis	Globorotalia crassaformis crassaformis	Other planktonic foraminifers	Vivianite nodules	Overall foraminifer abundance	Preservation	Abundance of bathyal benthic foraminifers	Abundance of abyssal benthic foraminifers	Comments	Ericson Zone	Age
155-939B-																																
1H-1, 27–29	0.27	0.29	C	C	B	F	C	F	B	C	C	B	B	B	C	R	B	B	B	B	B	B	B	B	B	A	G	B	B		Z	Holocene
1H-1, 82–84	0.82	0.84	B	F	B	F	C	B	B	C	C	B	R	B	F	B	B	B	B	R	B	B	B	B	B	A	G	B	B	PT,SP,RN	Z	Holocene
1H-1, 130–134	1.30	1.34	B	B	F	B	F	C	B	C	C	B	F	B	B	B	B	B	B	B	B	B	B	B	B	F	G	B	R	BN,M,PT	Y	late Pleist.
1H-CC, 5–14	3.90	3.99	F	C	B	F	F	R	B	C	C	B	C	B	F	B	B	B	B	B	B	B	B	B	B	C	G	B	B	RN	Y	late Pleist.
2H-CC, 43–52	13.33	13.42	B	R	B	C	F	B	B	B	C	B	B	B	C	B	B	B	B	B	B	B	B	B	F	R	M	B	B	PT,RN,BN,M	Y	late Pleist.
3H-CC, 5–14	23.83	23.92	B	B	B	B	C	B	B	C	C	B	B	B	C	B	B	B	B	B	B	B	B	B	C	R	M	B	B	IS,RN,BN,SP	Y	late Pleist.
4H-CC, 14–23	33.03	33.12	B	B	B	B	C	B	B	C	C	B	B	B	C	B	B	B	B	B	B	B	B	B	C	R	M	B	B	IS,RN,BN,SP	Y	late Pleist.
5H-CC, 63–72	42.98	43.07	B	B	B	B	F	B	B	A	C	B	B	B	C	B	B	B	B	B	B	B	B	B	A	R	G	B	B	SF,RN	Y	late Pleist.
6H-CC, 33–42	52.19	52.28	B	B	B	B	C	R	B	C	C	B	B	B	C	B	B	B	B	B	B	B	B	B	A	R	G	B	R	BN,SP	Y	late Pleist.
7H-CC, 45–54	61.91	62.00	R	B	B	B	C	R	B	C	C	B	R	B	C	B	B	B	B	B	B	B	B	B	A	F	G	B	B	BN,SP	Y	late Pleist.
8H-CC, 54–63	68.89	68.98	B	B	B	B	F	B	B	A	C	B	F	B	F	B	B	B	R	B	B	B	B	B	A	R	G	B	B	M,SP	Y	late Pleist.
9H-CC, 47–56	80.33	80.42	B	B	B	B	C	F	B	A	F	B	F	B	F	B	B	B	R	B	B	B	B	B	A	F	M	B	B	IS,M,SP	Y	late Pleist.
10X-CC, 0–9	87.40	87.49	B	B	B	B	C	B	B	A	C	B	B	B	C	B	B	B	B	B	B	B	B	B	A	R	M	B	B	PT,M,IS	Y	late Pleist.
11X-CC, 0–9	97.77	97.86	B	B	B	B	R	B	B	R	B	B	B	B	B	B	B	B	B	R	B	B	B	B	A	R	P	B	B	M	Y	late Pleist.

Notes: Key to Comments section: Sediment composition: PT = pteropods, S = sand, M = mica, BN = black nodules, RN = red nodules, AM = authigenic minerals; indicators of reworking: SF = shell fragments, W = wood fragments, SP = sponge spicules or spines, IS = iron-stained foraminifers. Note also the occurrence of bathyal benthic foraminifers.

Table 6. Spores and pollen data for Hole 939A.

Core, section, interval (cm)	Top interval (mbsf)	Bottom interval (mbsf)	Pollen and spores			Dinocysts	Wood/ carbonized particles	Ericson Zone (inferred from forams)	Age (inferred from forams)
			Abundance	Preservation	Major types recorded				
155-939A-									
2H-CC, 32–33	17.62	17.63	r	m	Euphorbiaceae	b	f	Y	late Pleist.
6H-CC, 123–124	56.85	56.86	f	m	Monolete spores, trilete spores	b	f	Y	late Pleist.
8H-CC, 14–15	74.26	74.27	r	p	Monosulcus	b	r	Y	late Pleist.
11X-CC, 22–23	96.21	96.22	b			b	r	Y	late Pleist.

Declination
(degrees)
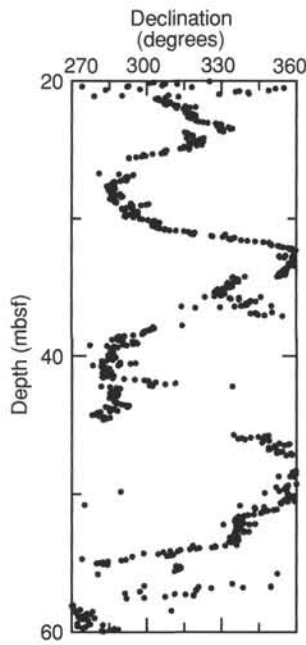

Figure 16. Azimuthally corrected declinations for interval of 20–60 mbsf in archive-half cores from Hole 939A. AF demagnetization level was 20 mT.

Hole 939A
Intensity (mA/m)

Hole 939B
Intensity (mA/m)

Figure 18. Remanence intensity of archive-half cores, after AF demagnetization to 20 mT, for 0–20 mbsf in Hole 939A and 0–100 mbsf in Hole 939B.

mbsf, the values in Hole 939C increase, to 11.0 mM at 37.00 mbsf, whereas the values in Hole 939B continue to decrease, reaching a minimum of 7.55 mM at 97.10 mbsf.

Sodium concentrations in Hole 939B are slightly higher than those in Hole 939C. With the exception of the values at 30 mbsf, the differences are not outside the analytical uncertainty of the measurements. In both holes, the sodium concentration decreases gradually downhole. The values are around 470 mM near the sediment surface and around 460 mM at 40 mbsf. Below 40 mbsf, the values are fairly constant.
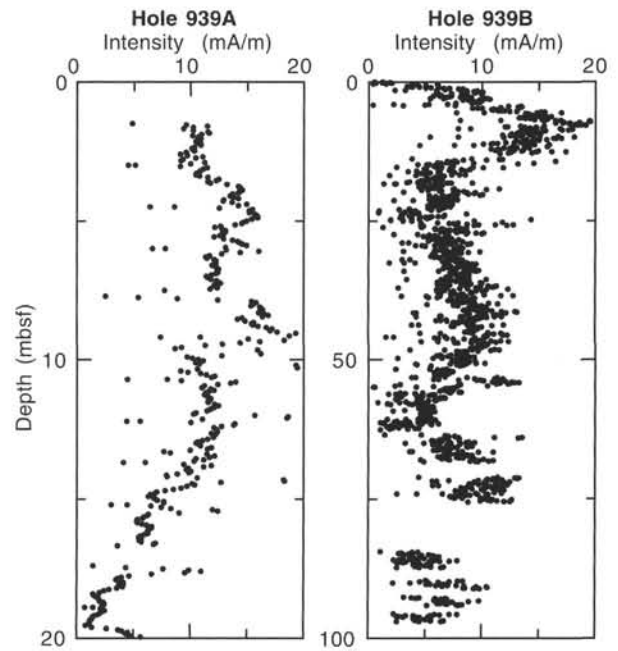
Dissolved iron concentrations in Hole 939C vary between 7.4 and 96 μM, with no clear trend downhole (Fig. 23M). In Hole 939B, the concentrations vary from 26.0 to 148.3 μM, again with no clear downhole trend. Below 10 mbsf in Hole 939C, the variations in iron concentration parallel changes in phosphate concentration.

Manganese concentrations are at a maximum of 37.2 μM at 0.20 mbsf, indicating anoxic conditions very near the sediment/water interface (Fig. 23N). Concentrations decrease to 16 μM at 1.45 mbsf and to less than 10 μM by 11.45 mbsf. Thereafter, the values are generally from 4 to 6 μM downhole.

Hole 939A
Inclination
(degrees)

Hole 939B
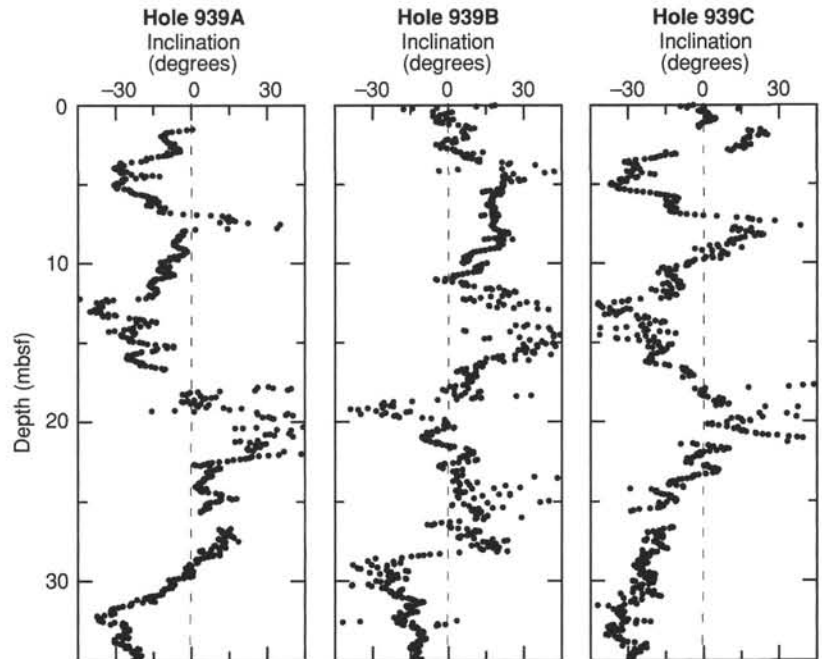Inclination
(degrees)

Hole 939C
Inclination
(degrees)

Figure 17. Comparison of the inclinations for the interval 0–35 mbsf in archive-half cores from Holes 939A, 939B, and 939C. AF demagnetization level was 20 mT.

Figure 19. The whole-core and discrete-sample magnetic susceptibilities for Hole 939B.

Sediment Geochemistry

Four mud samples of the Amazon levee were analyzed for major- and trace-element geochemistry (Tables 10 and 11). Mud compositions are similar to those of previous sites, with SiO_2 varying from 61 to 63 wt%, Al_2O_3 between 21 and 22 wt%, and CaO abundances between 0.7 and 0.9 wt%. Element ratios are also similar to those of previous sites, with K_2O/Al_2O_3 of 0.14 and Na_2O/Al_2O_3 of 0.06 to 0.07. The chemical composition is consistent with a mineralogy dominated by terrigenous silicates.

PHYSICAL PROPERTIES

Index Properties

Index properties were measured only for lithologic Unit II (0.68–99.4 mbsf) in Hole 939B (Table 12). Water content decreases with depth in the clay and silty clay of Unit II from 50% at 1.86 mbsf to 29% at 97.55 mbsf (Fig. 25). The uniform downhole decrease is interrupted by an interval between 17 and 27 mbsf in which water content is nearly constant at 36%. Below 27 mbsf, water content decreases relatively uniformly through Core 939B-10X. Core 939B-11X, the lowermost core in Hole 939B, is marked by two intervals (90.15–93.66 mbsf and 95.10–97.55 mbsf) over which porosity decreases 2%–3% with depth. It is unclear whether this variation represents lithologic changes or coring disturbance. The variation is not consistent with the assumed coring disturbance pattern in XCB cores at Sites 932, 937, and 938, which is characterized by a more continuous porosity decrease over the length of individual cores.

Fluctuations similar to those of water content are evident in the porosity and wet-bulk density profiles (Fig. 25). In Hole 939B, the porosity and wet-bulk density change downhole from 72% to 51% and 1.52 to 1.88 g/cm^3, respectively. Between 17 and 27 mbsf, porosity and wet-bulk-density are nearly constant with values of approxi-
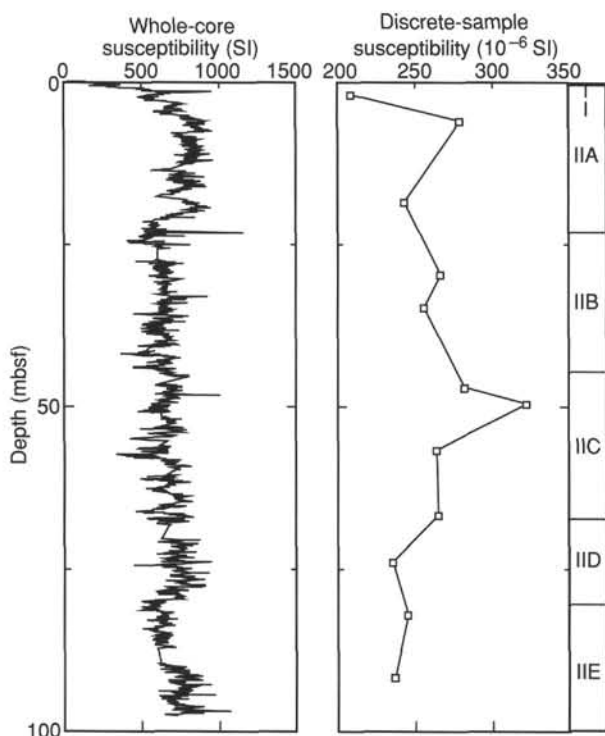
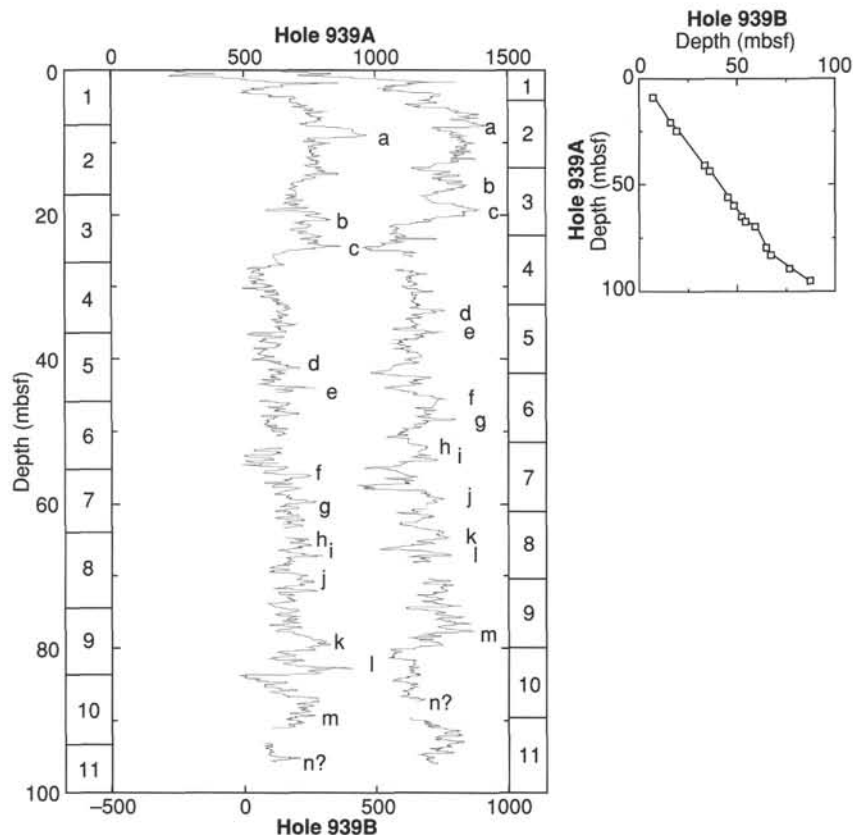Figure 20. A proposed correlation scheme between Holes 939A (left plot) and 939B (right plot) using the magnetic susceptibility profiles. The locations of core boundaries are shown on the outer portion of the figure. The scale for the susceptibility data from Hole 939B is at the bottom of the figure.

Table 7. Gas concentrations in sediments from Site 939.

Core, section, interval (cm)	Depth (mbsf)	Sed. temp.* (°C)	Methane	
			HS (ppm)	VAC (ppm)
155-939A-				
1H-1, 0–5	0.00	2	5	
2H-7, 0–5	16.70	3	33,270	
3H-2, 0–5	17.41	3	14,873	73,968
4H-7, 0–5	35.70	3	10,047	337,117
5H-2, 0–5	37.70	3	6,550	402,486
6H-7, 0–5	53.73	4	8,411	212,888
7H-2, 0–5	56.70	4	10,412	251,000
8H-3, 0–5	67.45	4	8,773	486,635
9H-3, 0–5	77.13	4	8,657	539,510
10X-3, 0–5	86.70	5	10,091	

Notes: HS = headspace; VAC = vacutainer. Geothermal gradient = 29°C/km. Bottom-water temperature = 2°C. *See "In-situ Temperature Measurements" section, this chapter.
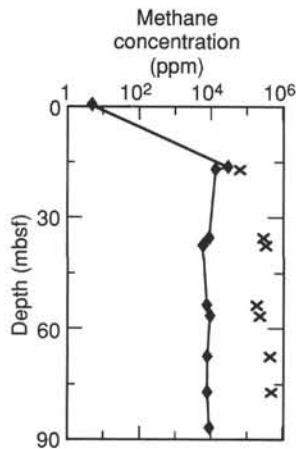

Figure 21. Methane concentrations at Site 939. Headspace (diamond) and vacutainer (×) samples are plotted.

mately 60% and 1.75 g/cm³. Grain density in Hole 939B ranges between 2.65 and 2.79 g/cm³ and averages 2.71 g/cm³.

The GRAPE bulk-density profile for Hole 939B differs from those of previous Amazon Fan sites in that there is a thicker interval at the top of the hole within which the GRAPE densities match the densities of the discrete samples (Fig. 25). The two data sets show good agreement from the seafloor through Section 939B-2H-5. Beginning in Section 939B-2H-6, the data sets rapidly diverge, exhibiting differences of 0.15 to 0.45 g/cm³, as the GRAPE densities are reduced as a consequence of gas-induced expansion.

Except for the interval of nearly constant water content, porosity, and wet-bulk density between 17 and 27 mbsf, the variation of bulk properties at Site 939 is typical of that of fine-grained terrigenous sediment undergoing gravitational compaction. The constancy of the properties in the 17 to 27 mbsf interval implies that normal consolidation has been inhibited. No specific changes are noted in the lithologic observations, nor among geochemical indicators for this interval. Anomalies that do coincide within the 17 to 27 mbsf interval are increased magnetic declination variability and a spectral reflectance shift toward shorter wavelength (green) values. The significance of the coincidence of these anomalies is not presently known.

Compressional-wave Velocity

Compressional-wave-velocity measurements were attempted on whole-round sections of cores from Holes 939A, 939B, and 939C and on split sections from Hole 939B. Because core expansion produced

pervasive microfractures in the sediment, neither the PWL nor DSV was capable of transmitting an acoustic signal through the sediment below Core 939B-2H. Seven longitudinal velocity measurements were made with the DSV between 1.86 and 10.35 mbsf (Table 13). Over this interval the velocity increases from 1497 to 1529 m/s and averages 1515 m/s. Transverse velocities were obtained by the PWL for the intervals of 0 to 7.45 mbsf in Hole 939A, 0 to 12.40 mbsf in Hole 939B, and 0 to 8.87 mbsf in Hole 939C. The average velocities for these three intervals are 1489, 1505, and 1494 m/s, respectively.

Shear Strength

Measurements of undrained shear strength were made using the motorized shear vane on all cores from Hole 939B (Table 14). Below 47 mbsf, compressive strengths were determined with a pocket penetrometer and used to estimate undrained shear strength.

Hole 939B (Fig. 26) is characterized by a slightly irregular increase in shear strength from 5.8 kPa at 1.86 mbsf to 22.3 kPa at 42.12 mbsf. Within this interval, the maximum shear strength is 29.4 kPa at 33.13 mbsf. Reduced strength (10.2–15.6 kPa) coincides with the interval of nearly constant bulk properties between 17 and 27 mbsf. Below 43 mbsf, shear strength variability increases. The strength increases from 37.9 kPa at 43.20 mbsf to a maximum of 50.4 kPa at 47.55 mbsf before varying irregularly to 42.4 kPa at the base of the hole. The shear strength measured by the lab vane and that estimated from the compressive strength are in very good agreement. At the base of the hole, the compressive strength estimate for undrained shear strength is 58.9 kPa.

The residual undrained shear strength also increases with depth in Hole 939B (Table 14), but at a lower rate than the peak strength. A slight downhole decrease in the residual/peak undrained shear strength ratio results from the difference in gradients.

Resistivity

Longitudinal and transverse resistivity were determined for cores from Hole 939B (Table 15). Longitudinal resistivity displays a general downhole increase that parallels the downhole decrease in porosity, but with slightly greater variability (Fig. 27). Resistivity increases from 0.27 Ωm near the seafloor to 0.38 Ωm at the base of Hole 939B. Comparison of longitudinal and transverse measurements indicates that the sediment resistivity is weakly anisotropic. The resistivity anisotropy averages –2.3% over the length of the hole and displays no clear lithologic or downhole trends (Fig. 27).

IN-SITU TEMPERATURE MEASUREMENTS

Temperature gradients and heat flow were determined using two downhole measurements and the bottom-water (mud-line) temperature. Two ADARA measurements were made during Cores 939B-6H (51.5 mbsf) and -9H (80 mbsf) using instrument number 12. The mud-line temperature of 2.75°C measured from this instrument was used as the reference bottom-seawater temperature at Site 939. Successful measurements resulted in extrapolated equilibrium temperatures of 4.1°C at 51.5 mbsf, and 5.1°C at 80 mbsf.

Equilibrium temperatures, extrapolated from synthetic curves constructed to fit transient temperature data, are plotted as a function of depth (mbsf) in Figure 28. Using the ADARA mud-line temperature and the sub-bottom temperatures from the two ADARA measurements downhole, the geothermal temperature gradient can be approximated by a linear mean of 29.4°C/km. We calculated heat flow by adopting the constant geothermal temperature gradient of 29.4°C/km and a linear increase in thermal conductivity, K, of 1.1 ± 0.15 W/(m·K), which is an average of regression estimates at 80 mbsf. This results in a calculated heat flow of 32.37 mW/m².

Table 8. Elemental and organic carbon compositions of sediments from Site 939.

| Core, section, interval (cm)	Depth (mbsf)	IC (%)	CaCO₃* (%)	TC (%)	TOC (%)	TN (%)	TS (%)	[C/N]a
155-939B-								
1H-1, 50–51	0.50	0.43	3.6	1.16	0.73	0.11	0.17	7
1H-1, 115–116	1.15	0.25	2.1	0.76	0.51	0.07	0.27	9
1H-2, 56–57	2.06	0.14	1.2	0.88	0.74	0.08	0.14	12
2H-3, 50–51	7.50	0.21	1.7	1.07	0.86	0.09	0.12	11
2H-5, 85–86	10.85	0.31	2.6	1.05	0.74	0.08	0.12	11
2H-6, 50–51	12.00	0.26	2.2	1.14	0.88	0.08	0.10	13
3H-4, 66–67	17.50	0.32	2.7	1.30	0.98	0.09	0.06	13
4H-6, 5–6	30.55	0.32	2.7	1.11	0.79	0.12	1.21	8
4H-6, 27–28	30.77	0.31	2.6	1.20	0.89	0.09	0.10	12
5H-2, 96–97	34.96	0.18	1.5	1.23	1.05	0.08	0.11	16
5H-6, 56–57	40.56	0.25	2.1	1.29	1.04	0.09	0.06	14
6H-5, 46–47	47.17	0.27	2.2	1.23	0.96	0.06	0.02	17
7H-7, 42–43	59.59	0.34	2.8	1.12	0.78	0.08	0.02	12
8H-5, 40–41	65.35	0.32	2.7	1.15	0.83	0.07	0.00	14
9H-5, 26–27	75.82	0.28	2.3	1.31	1.03	0.09	0.00	14
10X-3, 36–37	83.36	0.26	2.2	1.22	0.96	0.07	0.00	15
11X-3, 48–49	93.18	0.30	2.5	1.30	1.00	0.09	0.03	14
155-939C-								
1H-1, 55–56	0.55	0.43	3.6	1.14	0.71	0.05	0.04	16
1H-1, 118–119	1.18	0.20	1.7	0.71	0.51	0.05	0.18	12
1H-2, 55–56	2.05	0.06	0.5	0.76	0.70	0.04	0.08	22
1H-2, 120–121	2.70	0.10	0.8	1.03	0.93	0.05	0.10	21
1H-3, 55–56	3.55	0.18	1.5	1.03	0.85	0.04	0.06	24
1H-3, 120–121	4.20	0.18	1.5	1.04	0.86	0.05	0.03	19
1H-4, 55–56	5.05	0.18	1.5	1.20	1.02	0.06	0.09	21
1H-4, 120–121	5.70	0.16	1.3	1.01	0.85	0.05	0.08	21
1H-5, 55–56	6.55	0.21	1.7	1.03	0.82	0.05	0.08	20
1H-5, 116–117	7.16	0.19	1.6	1.06	0.87	0.07	0.10	16
2H-1, 49–50	8.09	0.20	1.7	1.06	0.86	0.04	0.07	26
2H-1, 90–91	8.50	0.33	2.7	1.19	0.86	0.04	0.00	26
3H-1, 30–31	17.40	0.23	1.9	1.19	0.96	0.09	0.10	12
3H-5, 30–31	23.00	0.29	2.4	1.30	1.01	0.10	0.08	11
4H-3, 29–30	29.89	0.28	2.3	1.22	0.94	0.10	0.06	11
4H-7, 40–41	36.00	0.28	2.3	1.01	0.73	0.08	0.04	10

Note: * = calculated assuming all IC is calcite.
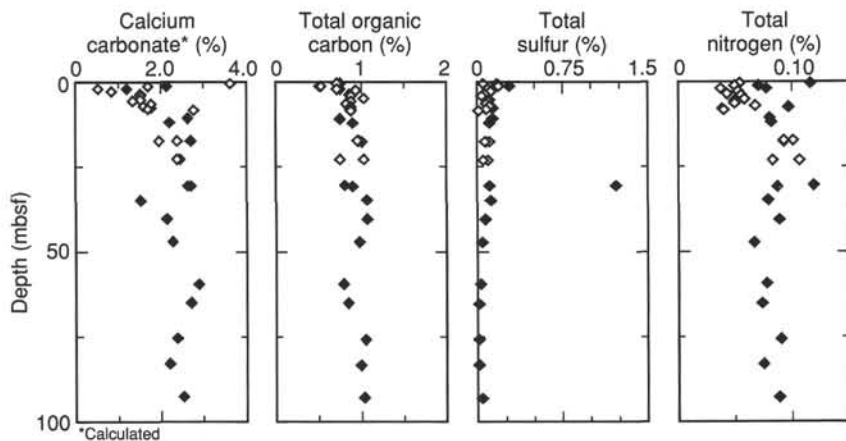
Figure 22. Concentration profiles of carbonate calculated as calcium carbonate, total organic carbon, total sulfur, and total nitrogen at Site 939. Solid symbols = data from Hole 939B; open symbols = data from Hole 939C.

SYNTHESIS AND SIGNIFICANCE

Stratigraphic Synthesis

Surficial Nannofossil-rich Clay (Unit I)

The 480-m offset of Holes 939A and 939B provided an opportunity to study lateral variability in upper-fan overbank turbidites. Hole 939B is taken as the type section for description of sub-bottom depths (Fig. 29). Unit I (0–0.68 mbsf) is a Holocene bioturbated foraminifer-nannofossil clay, underlain by an iron-rich crust and a gray nannofossil-rich clay.

Amazon-Brown Levee (Unit II)

The holes penetrated the upper 100 m of the levee of the Amazon-Brown-Aqua channels, which are coincident at this point. Total levee thickness, estimated from seismic reflection profiles, is about 250 m.

The base of the interval equivalent to the Brown levee is estimated at about 95 mbsf (Pirmez, 1994).

Unit II (0.68–99.40 mbsf) consists of mud with interbedded laminae and beds of silt and very fine sand. The mud has a carbonate content of <3%. Most of the unit is stained by diagenetic hydrotroilite in irregular patches or color bands. Small soft nodules of hydrotroilite, 1–2 mm in diameter, are common, and larger concretions and continuous bands are present from 8 to 16 mbsf. Unit II is subdivided into five subunits, based mainly on the frequency of silt laminae and beds. Subunit IIA (0.68–23.00 mbsf) comprises bioturbated mud. A prominent change in reflection character seen at 15 mbsf on 3.5-kHz profiles (R1 in Fig. 2) appears to form a seismic discontinuity, but has no corresponding lithologic change other than common 1- to 2-cm hydrotroilite nodules. Subunit IIB (23.00–44.23 mbsf) consists of moderately bioturbated mud with laminae and thin beds of silt. Burrows cut and obliterate parts of silt layers. Subunit IIC (44.23–66.17 mbsf) consists mainly of moderately bioturbated mud, with one short inter-

Table 9. Interstitial water chemistry, Site 939.

Core, section, interval (cm)	Depth (mbsf)	Salinity	pH	Alkalinity (mM)	Cl⁻ (mM)	Mg²⁺ (mM)	Ca²⁺ (mM)	K⁺ (mM)	HPO₄²⁻ (µM)	SO₄²⁻ (mM)	NH₄⁺ (mM)	H₄SiO₄ (µM)	Na⁺ (mM)	Fe²⁺ (µM)	Mn²⁺ (µM)
155-939B-															
1H-1, 145–150	1.45	35.0	7.71	12.82	551	49.3	10.7	13.1	29.5	21.0	0.8	303	472	44.1	13.2
2H-5, 145–150	11.45	34.0	7.70	33.29	556	46.2	7.8	9.9	97.7	0.1	2.4	405	469	26.0	10.0
3H-5, 150–155	19.84	34.0	7.73	23.37	557	44.3	5.9	9.5	30.0	0.6	3.9	374	467	48.2	6.0
4H-5, 145–150	30.45	33.5	7.51	24.61	557	42.2	5.1	8.7	13.4	0.2	5.2	394	474	88.2	5.6
5H-5, 145–150	39.95	33.0	7.55	11.48	557	41.7	5.0	8.0	7.8	0.7	5.5	388	462	69.4	4.8
7H-6, 140–150	59.07	32.5	7.19	6.38	561	43.5	4.1	7.6	4.3	0.5	6.6	327	459	148.3	5.6
9H-5, 140–150	76.96	32.5	7.42	10.53	562	45.2	4.3	7.3	4.3	0.3	6.8	392	460	52.5	4.4
11X-5, 140–150	97.10	32.5	7.46	9.11	564	43.5	4.5	7.6	3.3	0.4	7.2	339	463	34.4	4.8
155-939C-															
1H-1, 20–25	0.20	35.0	7.55	4.70	552	54.7	12.0	13.0	32.7	27.0	0.1	256	464	7.4	37.2
1H-1, 140–145	1.40	35.0	7.58	11.55	552	51.1	10.5	13.1	41.8	20.4	0.6	360	468	48.0	16.4
1H-2, 140–145	2.90	34.0	7.63	16.17	553	49.7	10.2	12.2	69.7	15.9	1.1	344	468	61.3	16.8
1H-3, 140–145	4.40	34.0	7.57	19.07	553	49.3	10.0	12.2	70.5	13.5	1.4	390	467	48.4	15.2
1H-4, 140–145	5.90	34.0	7.57	22.72	555	49.2	9.6	11.8	83.0	11.5	1.9	400	470	33.8	13.6
1H-5, 140–145	7.40	34.0	7.62	23.70	556	48.9	9.4	11.4	97.7	9.6	2.2	406	469	44.4	12.0
2H-1, 140–145	9.00	33.5	7.70	31.56	556	47.1	8.0	10.5	54.9	0.4	2.9	363	465	20.6	7.2
2H-2, 140–145	10.50	33.5	7.58	28.48	556	46.4	7.6	10.3	46.6	1.1	3.5	375	465	74.2	5.6
2H-3, 140–145	12.00	33.5	7.68	28.17	556	45.9	7.2	10.4	26.8	1.0	3.6	349	466	30.4	6.4
2H-4, 140–145	13.50	33.0	7.75	27.83	555	46.2	6.7	11.0	38.6	0.2	3.9	363	463	55.7	5.2
2H-5, 140–145	15.00	33.0	7.65	25.40	556	46.5	6.4	10.2	46.6	0.2	4.1	355	462	77.8	5.6
2H-6, 140–145	16.50	33.0	7.75	21.27	557	43.2	5.5	10.6	12.3	0.2	5.1	186	465	10.8	4.8
2H-7, 140–145	18.00	33.0	7.63	22.68	555	44.3	5.7	10.0	17.4	0.4	5.0	269	464	16.6	4.0
3H-1, 140–145	18.50	33.0	7.62	19.34	558	44.2	5.6	11.4	22.3	0.8	5.4	272	462	53.3	4.8
3H-3, 140–145	21.10	33.0	7.59	16.47	557	43.7	5.4	9.6	27.7	1.2	5.7	307	463	73.4	4.4
3H-5, 140–145	24.10	33.0	7.57	15.26	557	43.9	5.3	9.1	31.6	0.4	5.5	349	460	96.2	4.4
4H-1, 140–145	28.00	32.5	7.54	13.01	557	43.5	5.0	8.9	13.8	1.2	5.1	311	461	61.2	3.6
4H-3, 140–145	31.00	32.5	7.62	12.38	558	43.5	5.0	10.3	10.2	0.8	5.7	285	459	55.7	4.0
4H-5, 140–145	34.00	32.5	7.68	11.10	558	41.2	4.4	10.8	6.6	0.4	6.3	169	461	12.5	4.8
4H-7, 140–145	37.00	32.5	7.76	10.56	558	43.1	4.7	11.0	6.5	0.7	6.2	161	457	10.3	4.4

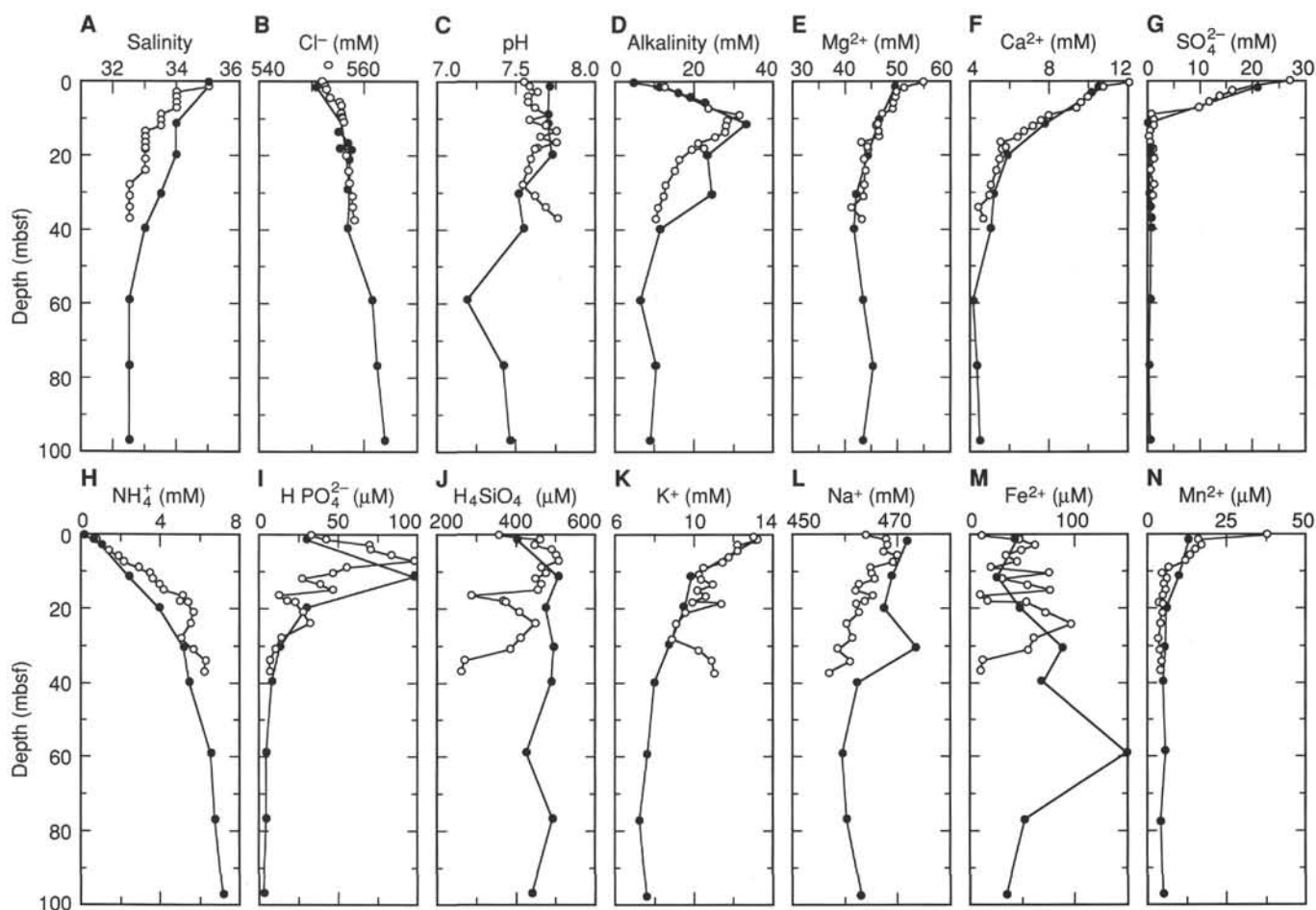Figure 23. Downhole variation in pore-water chemistry for Holes 939B (solid circles) and 939C (open circles): **A.** Salinity. **B.** Chloride. **C.** pH. **D.** Alkalinity. **E.** Magnesium. **F.** Calcium. **G.** Sulfate. **H.** Ammonium. **I.** Phosphate. **J.** Silica. **K.** Potassium. **L.** Sodium. **M.** Iron. **N.** Manganese.
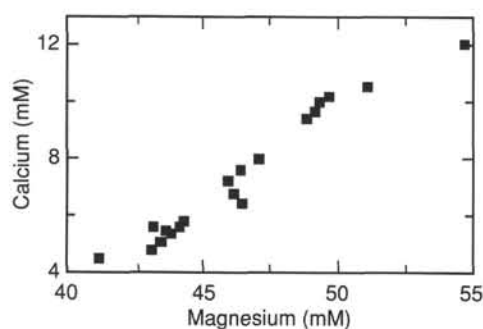
Figure 24. Calcium vs. magnesium concentrations for Hole 939C.

val with many silt laminae. Subunit IID (66.17–81.50 mbsf) resembles Subunit IIB, except for a greater frequency of silt laminae and beds. Subunit IIE (81.50–99.4 mbsf) consists of mud with some color banding, rare silt laminae, and structureless mud turbidites.

Implications

Foraminifer abundances are generally low below Subunit IIA. *P. obliquiloculata* is not present below the Holocene, indicating an age <40 ka for Unit II. No paleomagnetic excursion was found at this site either. These observations are consistent with the seismic stratigraphy of the site. The total thickness of the Amazon-Brown-Aqua levee at this site is about 250 m. If an age of 12 ka is assumed for the top and 22 ka for the base of this levee (based on extrapolation of sediment thicknesses above the regional Lake Mungo Excursion in Sites 930, 933, and 938), then mean sedimentation rate is about 25 m/k.y.

In Hole 939A, between 3 and 35 mbsf, a clear record of the variation in magnetic inclination, interpreted as secular variation, has a short 1- to 2-m wavelength variation superimposed on a longer 8- to 20-m wavelength variation. This variation can be correlated to the other two holes. In addition, there are three well-defined oscillations in declination over a range of 80° from 20 to 60 mbsf and two oscillations of <35° between 70 and 80 mbsf.

The 480-m offset of Holes 939A and 939B provided an opportunity to examine the reliability of various techniques for correlating between holes. The sediment sequence thickens toward the levee crest, and lithostratigraphic boundaries near the bottom of Hole 939A are about 13 m deeper than in Hole 939B. Both the number and thickness of silt beds decreases away from the channel. The bioturbation

of much of Unit II, however, hinders detailed lithologic correlation so that during the leg we were only able to correlate packets of silt laminae and beds from one hole to another and not individual beds. Correlation at a similar level of resolution can also be made with distinctive variation in magnetic susceptibility (Table 2) and paleomagnetic inclination.

Wet-bulk density increases abruptly at 15 and 28 mbsf and then decreases or remains constant downcore (best shown from 15 to 27 mbsf and less clearly from 28 to 32 mbsf in Hole 939B; Fig. 25). These intervals have correspondingly low shear strength and correspond to mottled mud with rare silt laminae. The horizons at which wet-bulk density increases correspond to two prominent reflections with toplap in the 3.5-kHz profiles (Figs. 2 and 3). The origin of the change in wet-bulk density that appears responsible for the reflections is unclear, and they do not correspond to any obvious sedimentological change. The change in wet-bulk density might result from variation in the distribution of diagenetic hydrotroilite.

At Hole 939C, interstitial waters were collected at 1.5-m intervals to 18.5 mbsf and thereafter at 3-m intervals to 37 mbsf. Samples were also taken every 20 m in Hole 939B. Magnesium and calcium decrease from 55 mM (Mg) and 12 mM (Ca) at 0.2 mbsf to about 43 mM (Mg) and 4 mM (Ca) near 30 mbsf, thereafter remaining almost constant. Mg and Ca concentrations correlate well, suggesting that their loss from the pore water is related. Pore-water sulfate diminishes from 27 mM at 0.2 mbsf to 21 mM at 1.4 mbsf and to zero by 9 mbsf. Alkalinity increases rapidly to 31 mM at 9 mbsf, decreases to 10 mM at 40 mbsf, and remains constant below that. Balancing possible sources and sinks of alkalinity suggests that almost all alkalinity removed from pore fluids can be accounted for as Ca or Mg carbonate. No discrete carbonate phases, however, have been identified in the cores, although chemical analysis shows 1%–3% carbonate in mud samples. Pore-water phosphate peaks at 98 mM, at the depth of complete sulfate reduction (9 mbsf). Dissolved iron is between 56 and 94 mM in the upper 33 mbsf, reaches a peak of 326 mM at 42 mbsf, and then decreases to 143 mM at 73 mbsf. Organic carbon ranges from 1.0% to 0.8% in Unit II. Vivianite (iron phosphate) nodules are common and displace surrounding sediment, crosscutting previously formed iron monosulfides that fill pore space. Organic carbon concentration is almost constant through the interval of detailed pore-water study. Slight changes in elemental compositions may be related to diagenetic changes, such as low nitrogen values at 0.5–8.0 mbsf, which could indicate preferential oxidation of reactive nitrogenous organic compounds. Shore-based analyses of more reactive organic fractions will be necessary to assess the effect of organic-matter diagenesis on pore-water chemistry and vivianite formation.

Table 10. Major element composition (wt%) of sediment samples, Site 939.

Core, section, interval (cm)	Depth (mbsf)	Lithology	SiO$_2$	TiO$_2$	Al$_2$O$_3$	Fe$_2$O$_3$	MnO	MgO	CaO	Na$_2$O	K$_2$O	P$_2$O$_5$	Total	LOI
155-939B-														
2H-5, 80–85	10.80	Mud	63.15	1.03	20.88	7.41	0.11	2.03	0.89	1.44	2.96	0.19	100.09	8.05
4H-6, 29–33	30.79	Mud	61.68	1.04	21.86	7.65	0.11	2.04	0.69	1.42	3.00	0.19	99.66	8.47
7H-7, 30–35	59.47	Mud	61.41	1.05	21.87	7.79	0.10	2.03	0.69	1.41	3.00	0.22	99.57	8.08
11X-3, 110–115	93.80	Mud	62.39	1.04	20.74	7.64	0.13	2.06	0.79	1.42	2.91	0.18	99.29	7.86

Notes: Total iron is reported as Fe$_2$O$_3$. LOI = loss on ignition.

Table 11. Trace element composition (ppm) of sediment samples, Site 939.

Core, section, interval (cm)	Depth (mbsf)	Lithology	Ba	Ce	Cr	Cu	Nb	Ni	Rb	Sr	V	Y	Zn	Zr
155-939B-														
2H-5, 80–85	10.80	Mud	477	104	60	32	20	32	127	156	85	40	119	233
4H-6, 29–33	30.79	Mud	475	107	66	33	22	33	132	142	86	40	124	220
7H-7, 30–35	59.47	Mud	486	108	70	34	22	37	133	142	93	39	124	228
11X-3, 110–115	93.80	Mud	480	103	65	31	22	32	127	149	85	41	122	232

Table 12. Index properties at Site 939.

Core, section, interval (cm)	Depth (mbsf)	Water content (%)	Wet-bulk density (g/cm³)	Grain density (g/cm³)	Dry-bulk density (g/cm³)	Porosity (%)	Void ratio
155-939B-							
1H-2, 35–37	1.85	50.0	1.52	2.65	0.76	72.2	2.59
1H-3, 35–38	3.35	45.0	1.60	2.76	0.88	68.8	2.20
2H-1, 43–45	4.43	42.1	1.62	2.65	0.93	65.3	1.89
2H-2, 34–36	5.84	42.0	1.67	2.75	0.97	66.0	1.94
2H-3, 34–36	7.34	40.2	1.66	2.66	1.00	63.6	1.74
2H-4, 34–36	8.84	40.2	1.64	2.68	0.98	63.7	1.75
2H-5, 34–36	10.34	38.4	1.69	2.69	1.04	62.1	1.64
2H-6, 34–36	11.84	37.7	1.74	2.72	1.08	61.6	1.61
3H-2, 34–36	14.20	36.4	1.73	2.72	1.10	60.3	1.52
3H-3, 34–36	15.68	35.1	1.78	2.72	1.16	59.0	1.44
3H-4, 38–40	17.22	36.0	1.75	2.68	1.12	59.5	1.47
3H-5, 38–40	18.72	35.9	1.74	2.69	1.12	59.5	1.47
3H-6, 38–40	20.27	36.1	1.76	2.72	1.13	60.0	1.50
3H-7, 38–40	21.77	36.1	1.76	2.77	1.12	60.5	1.53
4H-1, 64–66	23.64	36.5	1.74	2.73	1.11	60.5	1.53
4H-2, 85–87	25.35	35.6	1.74	2.69	1.12	59.1	1.45
4H-3, 82–84	26.82	36.3	1.73	2.65	1.10	59.6	1.47
4H-4, 80–82	28.30	34.0	1.78	2.69	1.18	57.5	1.35
4H-5, 82–84	29.82	34.4	1.78	2.69	1.17	57.9	1.38
4H-6, 78–80	31.28	32.8	1.77	2.67	1.19	56.1	1.28
4H-7, 59–61	32.59	33.5	1.79	2.70	1.19	57.0	1.33
5H-1, 62–64	33.12	32.6	1.81	2.74	1.22	56.4	1.29
5H-2, 64–66	34.64	33.9	1.79	2.71	1.18	57.6	1.36
5H-3, 70–72	36.20	33.6	1.79	2.72	1.19	57.3	1.34
5H-4, 70–72	37.70	33.8	1.80	2.73	1.19	57.7	1.36
5H-5, 96–98	39.46	33.3	1.81	2.71	1.20	56.9	1.32
5H-6, 66–68	40.66	33.1	1.80	2.71	1.20	56.7	1.31
5H-7, 61–63	42.11	32.2	1.81	2.67	1.23	55.3	1.24
6H-2, 98–100	43.19	33.3	1.79	2.66	1.19	56.5	1.30
6H-3, 83–85	44.54	33.2	1.81	2.73	1.21	57.0	1.33
6H-4, 83–85	46.04	34.3	1.78	2.74	1.17	58.3	1.40
6H-5, 83–85	47.54	32.5	1.81	2.66	1.22	55.6	1.25
6H-6, 58–60	48.79	32.5	1.82	2.66	1.23	55.5	1.25
6H-7, 85–87	50.56	32.2	1.83	2.67	1.24	55.4	1.24
6H-8, 29–31	51.50	31.0	1.87	2.73	1.29	54.5	1.20
7H-2, 67–69	52.34	31.7	1.85	2.75	1.26	55.5	1.25
7H-3, 76–78	53.93	32.3	1.81	2.68	1.23	55.5	1.25
7H-4, 88–90	55.55	31.6	1.82	2.71	1.25	55.1	1.23
7H-5, 62–64	56.79	32.6	1.81	2.69	1.22	55.9	1.27
7H-6, 63–65	58.30	31.0	1.85	2.75	1.27	54.7	1.21
7H-7, 74–76	59.91	30.9	1.83	2.72	1.27	54.3	1.19
7H-8, 47–49	61.14	30.2	1.85	2.76	1.29	53.9	1.17
8H-1, 84–86	61.84	31.0	1.84	2.77	1.27	54.9	1.22
8H-4, 79–81	64.24	30.4	1.85	2.73	1.29	53.9	1.17
8H-5, 90–92	65.85	31.7	1.82	2.73	1.25	55.2	1.23
8H-6, 84–86	67.29	30.1	1.88	2.74	1.31	53.5	1.15
8H-7, 24–26	68.19	30.9	1.86	2.77	1.29	54.7	1.21
9H-2, 100–102	72.06	30.5	1.87	2.78	1.30	54.4	1.19
9H-3, 90–92	73.46	30.1	1.86	2.70	1.30	53.1	1.13
9H-4, 90–92	74.96	30.6	1.86	2.70	1.29	53.7	1.16
9H-5, 87–89	76.43	29.6	1.88	2.75	1.33	53.1	1.13
9H-6, 73–75	77.79	29.4	1.88	2.75	1.32	52.8	1.12
9H-7, 101–103	79.57	29.0	1.87	2.69	1.33	51.8	1.08
10X-1, 65–67	80.65	31.8	1.83	2.79	1.25	55.9	1.27
10X-2, 83–85	82.33	30.3	1.88	2.79	1.31	54.2	1.18
10X-3, 98–100	83.98	30.5	1.88	2.77	1.31	54.2	1.18
10X-4, 73–75	85.23	30.3	1.88	2.74	1.31	53.8	1.16
10X-5, 90–92	86.90	30.7	1.84	2.71	1.28	53.9	1.17
11X-1, 45–47	90.15	31.6	1.83	2.70	1.25	54.9	1.22
11X-2, 102–104	92.22	29.8	1.86	2.72	1.31	52.9	1.12
11X-3, 96–98	93.66	28.4	1.89	2.71	1.36	51.2	1.05
11X-4, 90–92	95.10	30.8	1.86	2.75	1.28	54.5	1.20
11X-5, 77–79	96.47	29.0	1.86	2.68	1.32	51.7	1.07
11X-6, 35–37	97.55	28.7	1.88	2.69	1.34	51.4	1.06

This site represents one of the highest near-surface sedimentation rates of Leg 155. The upper part of the pore-water profile (to 5 mbsf) is similar to that at Site 931, where the sedimentation rate is several times lower, but the peaks in phosphate and iron are several meters deeper than at Site 931. Fluctuations in the deposition of silt beds on the upper fan occur with a period estimated to be on the order of hundreds to a few thousands of years.

REFERENCES

Damuth, J.E., 1977. Late Quaternary sedimentation in the western equatorial Atlantic. *Geol. Soc. Am. Bull.*, 88:695–710.

Pirmez, C., 1994. Growth of a submarine meandering channel-levee system on the Amazon Fan [Ph.D. thesis]. Columbia Univ., New York.

Ms 155IR-115

NOTE: For all sites drilled, core-description forms ("barrel sheets") and core photographs can be found in Section 4, beginning on page 703. Forms containing smear-slide data can be found in Section 5, beginning on page 1199. GRAPE, index property, magnetic susceptibility, and natural gamma data are presented on CD-ROM (back pocket).
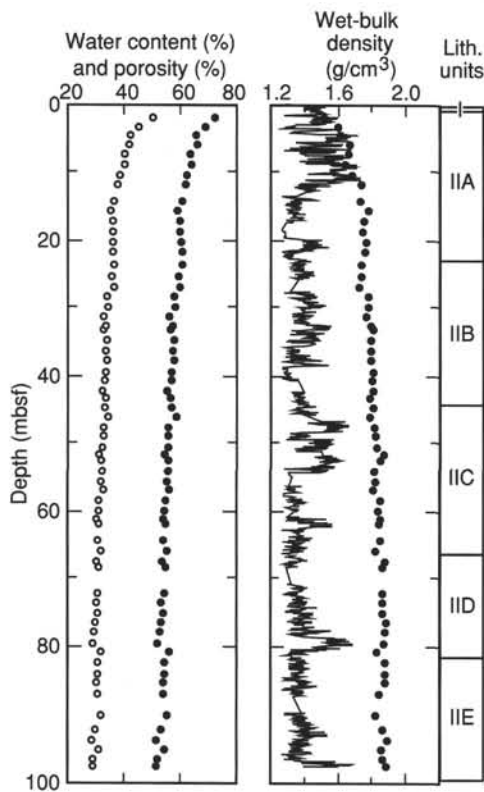
Figure 25. Water content (open circles) and porosity (solid circles), and wet-bulk density as determined for discrete samples and by the GRAPE (line) in Hole 939B.

Table 13. DSV compressional-wave velocity at Site 939.

Core, section, interval (cm)	Depth (mbsf)	Velocity (m/s)
155-939B-		
1H-2, 32–40	1.86	1497
1H-3, 32–41	3.36	1507
2H-1, 40–48	4.44	1516
2H-2, 31–39	5.85	1515
2H-3, 31–40	7.35	1519
2H-4, 31–41	8.85	1524
2H-5, 31–42	10.35	1529

Note: All measurements are in the longitudinal direction.

Table 14. Undrained shear strength at Site 939.

Core, section, interval (cm)	Depth (mbsf)	Peak undrained shear strength (kPa)	Residual undrained shear strength (kPa)	Unconfined compressive strength* (kPa)
155-939B-				
1H-2, 36	1.86	5.8	4.5	
1H-3, 36	3.36	6.8	4.9	
2H-1, 44	4.44	7.2	5.4	
2H-2, 35	5.85	10.2	7.2	
2H-3, 35	7.35	12.6	8.8	
2H-4, 35	8.85	13.5	9.4	
2H-5, 35	10.35	15.0	10.0	
2H-6, 35	11.85	13.1	9.1	
3H-2, 35	14.21	16.2	12.6	
3H-3, 35	15.69	11.5	8.2	
3H-4, 35	17.19	12.7	9.6	
3H-5, 39	18.73	10.2	8.0	
3H-6, 39	20.28	14.7	10.2	
3H-7, 39	21.78	14.1	10.4	
4H-1, 65	23.65	12.7	10.6	
4H-2, 86	25.36	15.6	10.7	
4H-3, 83	26.83	11.3	8.0	
4H-4, 81	28.31	17.0	12.8	
4H-5, 83	29.83	9.9	5.1	
4H-5, 92	29.92	14.1	9.0	
4H-6, 79	31.29	16.4	11.2	
4H-7, 60	32.60	19.0	13.2	
5H-1, 63	33.13	29.4	18.8	
5H-2, 65	34.65	26.6	16.6	
5H-3, 71	36.21	23.2	12.2	
5H-4, 71	37.71	23.8	8.0	
5H-5, 97	39.47	23.5	12.4	
5H-6, 67	40.67	24.6	15.5	
5H-7, 62	42.12	22.3	14.5	
6H-2, 99	43.20	37.9	20.8	
6H-3, 84	44.55	42.2	21.8	
6H-4, 84	46.05	28.6	18.2	
6H-5, 84	47.55	50.4	25.3	93.2
6H-6, 59	48.80	42.2	21.7	78.5
6H-7, 86	50.57	36.2	18.1	68.6
6H-8, 30	51.51	20.1	12.5	58.8
7H-2, 68	52.35	38.2	21.1	78.5
7H-3, 77	53.94	27.4	15.4	53.9
7H-4, 89	55.56	35.6	19.3	78.5
7H-5, 63	56.80	18.7	10.9	49.0
7H-6, 64	58.31	25.7	15.3	58.8
7H-7, 75	59.92	27.2	17.2	58.8
7H-8, 48	61.15	20.7	11.2	49.0
8H-1, 85	61.85	22.9	16.6	49.0
8H-4, 80	64.25	24.0	16.0	68.6
8H-5, 91	65.86	27.7	17.6	49.0
8H-6, 85	67.30	29.1	19.1	73.5
8H-7, 25	68.20	32.0	20.4	78.5
9H-2, 101	72.07	30.0	16.2	98.1
9H-3, 91	73.47	24.9	8.3	98.1
9H-4, 91	74.97	30.0	19.0	93.2
9H-5, 88	76.44	43.0	23.9	98.1
9H-6, 74	77.80	36.2	18.2	98.1
9H-7, 102	79.58	33.1	20.9	78.5
10X-1, 66	80.66	20.4	14.6	34.3
10X-2, 84	82.34	28.9	17.6	73.5
10X-3, 99	83.99	36.2	20.3	68.6
10X-4, 74	85.24	35.9	21.8	73.5
10X-5, 91	86.91	30.3	20.0	68.6
11X-1, 46	90.16	23.8	14.7	49.0
11X-2, 103	92.23	41.0	24.9	88.3
11X-3, 97	93.67	42.7	24.8	88.3
11X-4, 91	95.11	24.0	15.3	58.8
11X-5, 78	96.48	32.0	18.6	88.3
11X-6, 36	97.56	42.4	25.7	117.7

Note: *Unconfined compressive strength (q_u) can be used to approximate undrained shear strength (S_u) by the relationship $q_u = 2S_u$.
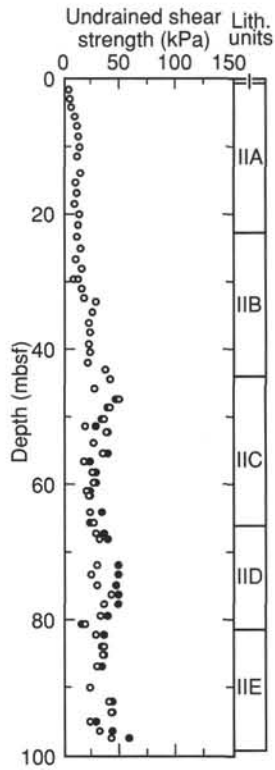
Undrained shear Lith.
strength (kPa) units

Figure 26. Undrained shear strength (open circles) and assumed undrained shear strength derived from unconfined compressive strength (solid circles) in Hole 939B.

Table 15. Electrical resistivity at Site 939.

| Core, section, interval (cm)	Depth (mbsf)	Longitudinal resistivity (Ωm)	Transverse resistivity (Ωm)
155-939B-			
1H-2, 36	1.86	0.283	0.253
1H-3, 36	3.36	0.270	0.248
2H-1, 44	4.44	0.278	0.270
2H-2, 35	5.85	0.271	0.272
2H-3, 35	7.35	0.293	0.281
2H-4, 35	8.85	0.298	0.290
2H-5, 35	10.35	0.297	0.307
2H-6, 35	11.85	0.326	0.316
3H-2, 35	14.21	0.318	0.317
3H-3, 35	15.69	0.334	0.341
3H-4, 35	17.19	0.328	0.318
3H-5, 39	18.73	0.339	0.315
3H-6, 39	20.28	0.337	0.324
3H-7, 39	21.78	0.347	0.326
4H-1, 65	23.65	0.342	0.347
4H-2, 86	25.36	0.339	0.326
4H-3, 83	26.83	0.328	0.335
4H-4, 81	28.31	0.346	0.356
4H-5, 83	29.83	0.353	0.335
4H-6, 79	31.29	0.369	0.357
4H-7, 60	32.60	0.345	0.348
5H-1, 63	33.13	0.341	0.342
5H-2, 65	34.65	0.335	0.327
5H-3, 71	36.21	0.332	0.318
5H-4, 71	37.71	0.339	0.344
5H-5, 97	39.47	0.344	0.349
5H-6, 67	40.67	0.349	0.336
5H-7, 62	42.12	0.367	0.364
6H-2, 99	43.20	0.352	0.330
6H-3, 84	44.55	0.328	0.327
6H-4, 84	46.05	0.338	0.340
6H-5, 84	47.55	0.370	0.335
6H-6, 59	48.80	0.358	0.339
6H-7, 86	50.57	0.346	0.328
6H-8, 30	51.51	0.383	0.384
7H-2, 68	52.35	0.369	0.346
7H-3, 77	53.94	0.352	0.344
7H-4, 89	55.56	0.337	0.329
7H-5, 63	56.80	0.355	0.343
7H-6, 64	58.31	0.356	0.357
7H-7, 75	59.92	0.350	0.364
7H-8, 48	61.15	0.357	0.356
8H-1, 85	61.85	0.400	0.348
8H-4, 80	64.25	0.391	0.377
8H-5, 91	65.86	0.353	0.377
8H-6, 85	67.30	0.417	0.385
8H-7, 25	68.20	0.413	0.406
9H-2, 101	72.07	0.374	0.338
9H-3, 91	73.47	0.347	0.346
9H-4, 91	74.97	0.344	0.340
9H-5, 88	76.44	0.332	0.329
9H-6, 74	78.00	0.342	0.337
9H-7, 102	80.00	0.277	0.266
10X-1, 66	80.66	0.329	0.324
10X-2, 84	82.34	0.338	0.332
10X-3, 99	83.99	0.324	0.306
10X-4, 74	85.24	0.343	0.333
10X-5, 91	86.91	0.329	0.342
11X-1, 46	90.16	0.307	0.329
11X-2, 103	92.23	0.337	0.352
11X-3, 97	93.67	0.363	0.357
11X-4, 91	95.11	0.385	0.329
11X-5, 78	96.48	0.331	0.320
11X-6, 36	97.56	0.323	0.343
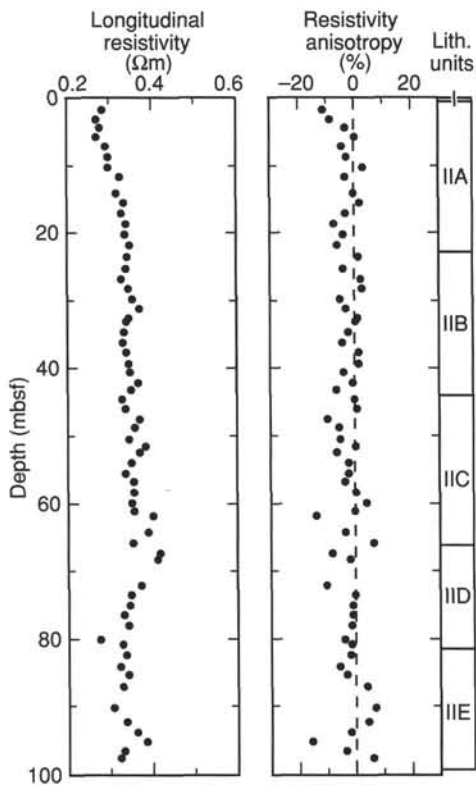
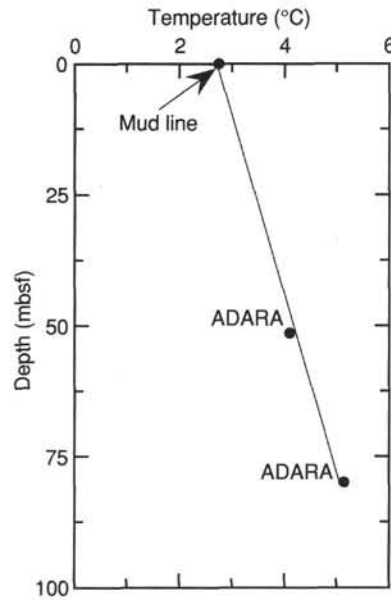Figure 27. Longitudinal resistivity and resistivity anisotropy in Hole 939B.

Figure 28. Estimated equilibrium temperatures in Hole 939B. A linear curve fit through the data suggests that reliable equilibrium temperatures were acquired that indicate a geothermal gradient of 29.43°C/km.
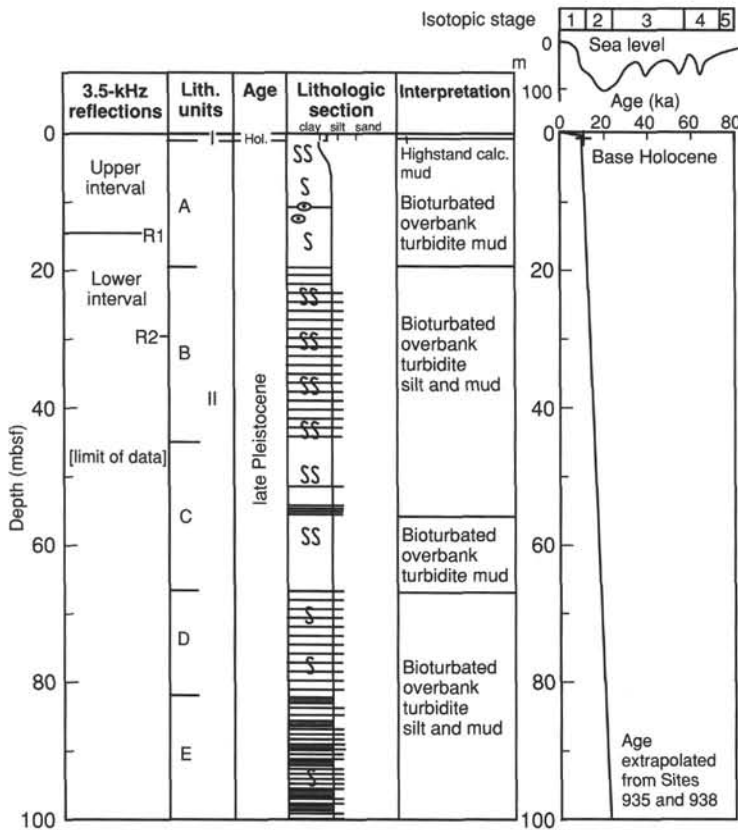

Figure 29. Summary of Site 939 showing acoustic stratigraphy, lithologic units, age, schematic lithologic column, interpreted sediment facies, chronological picks, and interpreted age-depth curve. Stippled pattern in lithologic section indicates thick mud turbidites.